Low Temperature Synthesis and Phosphorescence of Methylcyanotriacetylene

Urszula Szczepaniak, Robert Kolos, Marcin Gronowski, Jean-Claude Guillemin, Claudine Crépin

Low Temperature Synthesis and Phosphorescence of Methylcyanotriacetylene

Published as part of The Journal of Physical Chemistry virtual special issue "W. Lester S. Andrews Festschrift"

Urszula Szczepaniak[a, b] *, Robert Kołos[b], Marcin Gronowski[b], Jean-Claude Guillemin[c], and Claudine Crépin[a]

[a] Institut des Sciences Moléculaires d'Orsay (ISMO), UMR8214, CNRS, Univ. Paris-Sud, Université Paris-Saclay, F-91405 Orsay, France

[b] Institute of Physical Chemistry, Polish Academy of Sciences, Kasprzaka 44/52, PL-01-224 Warsaw, Poland

[c] Institut des Sciences Chimiques de Rennes, École Nationale Supérieure de Chimie de Rennes, CNRS, UMR 6226, 11 Allée de Beaulieu, CS 50837, 35708 Rennes Cedex 7, France

[*] e-mail : *uszczepaniak@ichf.edu.pl, urszula.szczepaniak@u-psud.fr*; Present address: Laboratory of Physical Chemistry, ETH Zürich, Vladimir-Prelog Weg 2, CH-8093 Zürich, Switzerland

ABSTRACT

This paper reports on UV-stimulated synthesis of methylcyanotriacetylene carried out in cryogenic rare gas matrices via coupling of smaller precursors: propyne and cyanodiacetylene. The detection was possible due to the strong visible $a\,^3A' \rightarrow X\,^1A_1$ phosphorescence of CH_3C_7N, discovered in the course of this work. The ensuing measurements of electronic spectroscopy revealed the formally forbidden $B\,^1E - X\,^1A_1$ system, as well as the allowed one $E\,^1A_1 - X\,^1A_1$, with origins at approx. 3.32 eV and 5.4 eV, respectively. It was also possible to revisit the spectroscopic characterization of cyanotriacetylene, HC_7N, formed in parallel to the title photoproduct. Spectral assignments were assisted with a density functional theory study.

INTRODUCTION

The $H(C{\equiv}C)_nCN$ molecules were observed with microwave spectroscopy, up to $n = 4$, in diverse extra-terrestrial sources.[1–6] Methylated cyanopolyacetylenes $CH_3(C{\equiv}C)_nCN$ are also of astrochemical interest; methylcyanoacetylene, CH_3C_3N, was identified in the Taurus Molecular Cloud (TMC)[7] and more recently in the Sagittarius B2 cloud near the Galactic center.[8] The presence of methylcyanodiacetylene, CH_3C_5N, in TMC has also been confirmed.[9,10,] This latter compound appears, along with CH_3C_3N and CH_3C_7N, in astrochemical kinetic models.[10–13] It may originate, according to Quan and Herbst,[10] from the dissociative recombination of $CH_3C_5NH^+$ cations with electrons or from the encounter of neutral species CN and CH_3C_4H. Markwick *et al.*[12] considered the reaction of HC_5N with $CH_3OH_2^+$. CH_3C_3N was also included in modelling of Titan's atmosphere[14,15], and indeed the mass-spectrometric data from Cassini spacecraft suggested the presence of both CH_3C_3N and CH_3C_5N.[14]

Addition of a methyl group to a cyanopolyacetylenic chain changes its physical properties. For example, we could see partial thermal decomposition of HC_5N occurring even at -78°C, while the methylated analogue, CH_3C_5N, remains stable at least its melting point (92°C [16]). The same trend was observed by us for HC_3N and CH_3C_3N: at room temperature, the condensed phase of the latter is stable while the former decomposes and has to be stored below -20°C.

The smallest of methylcyanopolyacetylenes, CH_3C_3N, has been the subject of numerous spectroscopic investigations.[17–24] For CH_3C_5N, the next member of the series, gas-phase rotational transitions[25,26] and infrared absorption[27] were reported, as well as vibrational[28] and electronic[29] spectra of pure solid and of rare gas matrix-isolated compound. It was reported that photolysis of $CH_3C{\equiv}CH$ (propyne) mixed with cyanoacetylene leads to CH_3C_5N.[16] Kerisit et al. [30]

suggested that CH_3C_7N might analogously form in photochemical reactions involving gaseous $CH_3C{\equiv}C\text{-}C{\equiv}CH$ (1,3-pentadiyne) and HC_3N precursors (the identification was based on a single ^1H NMR peak).

The first report to mention CH_3C_7N (methylcyanotriacetylene, 6-methyl-1-cyanohexa-1,3,5-triyne, octa-2,4,6-triynenitrile) discussed its difficult synthesis, and provided infrared, as well as UV absorption spectra (for an ether solution).[31] Microwave transitions were subsequently investigated.[26,32,33] Theoretical results are available for rotational constants, molecular geometry, polarizability, and electric dipole moment.[34,35]

Our earlier studies [36–38] demonstrated the appearance of mono- and dicyanopolyacetylenes in cryogenic UV-stimulated processes, out of shorter $H(C{\equiv}C)_nCN$ species reacting with one another or with acetylenic-type molecules $H(C{\equiv}C)_mH$. Such syntheses have already been shown to work for cyanodiacetylene (HC_5N),[36,38] cyanotriacetylene (HC_7N),[37] and cyanotetraacetylene (HC_9N).[39] In particular, HC_7N was detected in UV-irradiated (H_2 discharge lamp or 193 nm laser) solid Ar doped with either $HC_3N + C_4H_2$ or $HC_5N + C_2H_2$ mixture.[37] HC_7N was also produced by electric discharges in a HC_3N/Kr mixture, prior to the trapping onto a cold substrate.[40] In all these cryogenic approaches, the generated cyanopolyacetylenes were found to emit strong phosphorescence, which proved to be the most sensitive spectroscopic indicator of their presence. However, no photochemically-stimulated cryogenic synthesis has as yet been reported for any methylated cyanopolyacetylene. Here we aimed at verifying the utility of such an approach to the formation of CH_3C_7N by coupling the precursors CH_3C_2H and HC_5N. Propyne, similarly to HC_5N, features an easily photodetachable acetylenic hydrogen atom.[41,42] The targeted molecule has indeed appeared along with HC_7N, offering an opportunity to compare

the electronic transitions of the two closely related products and to extend the prior knowledge on UV-Vis absorption[43–46] and low temperature phosphorescence[37,40] of HC_7N. Spectroscopic assignments were backed with density functional theory calculations of electronic and vibrational energy levels.

METHODS

A. Experimental

Propyne was commercially available from Aldrich (purity > 97%). The second precursor, cyanodiacetylene, was prepared using the method developed by Trolez & Guillemin.[47] The compounds were purified before the experiments by pumping while kept at T<200 K (HC_5N) or by several freeze-pump-thaw cycles with freezing at T<200 K (CH_3C_2H).

Krypton (purity 4.0, Messer), mixed with the precursor chemicals, was trapped onto a sapphire substrate held at 30 K inside a closed-cycle helium cryostat. Photochemical transformations were induced with a 193 nm ArF excimer laser. All details concerning the experimental set-up and spectroscopic instrumentation were given in a paper by Szczepaniak et al. (this issue).[39] Experiments were primarily aimed at identification of the created photoproducts and characterization of their electronic transitions, by measuring dispersed phosphorescence spectra, as well as phosphorescence excitation spectra, and phosphorescence lifetime.

An experiment involving CH_3C_2H + HC_3N mixture (HC_3N obtained following the Miller and Lemon[48] method), expected to yield CH_3C_5N, was first performed to verify the validity of the applied approach. The test was positive; not only the phosphorescence of CH_3C_5N, but also that

of HC_5N could be detected in $Kr/CH_3C_2H/HC_3N$ (1000/1/1) matrices previously subjected to 193 nm photolysis.

Two different gas mixtures were used in the main CH_3C_2H + HC_5N experiment. Cyanodiacetylene was deposited in the amount either the same or twice smaller than that of propyne. The latter mixture ($Kr/CH_3C_2H/HC_5N$ ratio of 1000/2/1) noticeably favored the formation of CH_3C_7N over HC_7N.

B. Computational details

Theoretical procedures applied here coincide with those described in more detail in a recent paper by Szczepaniak et al.[39] GAUSSIAN 09 (Rev. B. 01)[49] implementations of the density functional theory (DFT)[50] were mostly applied. The B3PW91[51] functional was employed in the derivation of molecular geometries, harmonic vibrational frequencies, IR absorption intensities, and Raman activities for the ground and the lowest triplet state, while the time-dependent B3PW91 approach served for predicting transitions from the ground to excited singlet electronic states. Basis set aug-cc-pVTZ[52,53] was applied in all these computations.

Geometry optimizations carried out for excited singlet states of CH_3C_7N led to the structures (genuine potential energy minima) very slightly deviating from the C_{3v} symmetry. Based on our former CH_3C_5N study,[29] we suppose this effect to be of a purely numerical nature.

Influence of the Herzberg–Teller effect on intensity of the vibronic $B\,^1\Delta - X\,^1\Sigma^+$ transitions was estimated by carrying out oscillator strength calculations for a HC_7N molecule slightly distorted, mimicking, case by case, the effect of various bending vibrations. The distortion vector was

always parallel to a respective normal coordinate and had a length of 0.1 Å. The coupling effect was considered as important when the described simulation produced a noticeable oscillator strength ($f \geq 0.0001$).

RESULTS AND DISCUSSION

A. Theoretical predictions

Despite obviously different molecular symmetries, HC_5N and CH_3C_5N exhibit strikingly alike electronic spectra, as noticed by Turowski et al.[29] Such similarities, stemming from closely related chromophores, were expected also for the HC_7N/CH_3C_7N pair. Quantum chemical predictions for the lowest electronic energy levels of HC_7N and CH_3C_7N are presented in Table 1; general patterns of electronic state distribution are indeed very similar for both species. Nevertheless, the states arising from HOMO-LUMO electronic excitations have slightly higher energies for HC_7N than for CH_3C_7N (resembling what was observed for HC_5N and CH_3C_5N).[29] For both molecules, $\tilde{E} - \tilde{X}$ is predicted as the strongest transition. The expected $\tilde{a} - \tilde{X}$ transition energy of CH_3C_7N (2.23 eV) is practically identical to that of HC_7N (2.25 eV), just as previously calculated and measured for CH_3C_5N and HC_5N (2.90 eV vs. 2.92 eV at CAM-B3LYP/aug-cc-pVTZ level of theory, 2.94 vs. 2.92 eV in Ar matrix).[29]

Table 1. Energy [eV], wavelength [nm], and oscillator strength for transitions involving the ground and excited electronic states of HC_7N and CH_3C_7N, as calculated at B3PW91/aug-cc-pVTZ level of theory. Electronic configurations of the molecules are the following. HC_7N, $X\ ^1\Sigma^+$: [core] $(1\sigma)^2\ (2\sigma)^2\ (3\sigma)^2\ (4\sigma)^2\ (5\sigma)^2\ (6\sigma)^2\ (1\pi)^4\ (7\sigma)^2\ (2\pi)^4\ (8\sigma)^2\ (9\sigma)^2\ (3\pi)^4\ (4\pi)^4\ (1\pi^*)^0\ (2\pi^*)^0\ (1\sigma^*)^0$; CH_3C_7N, $X\ ^1A_1$: [core] $(1a_1)^2\ (2a_1)^2\ (3a_1)^2\ (4a_1)^2\ (5a_1)^2\ (6a_1)^2\ (7a_1)^2\ (1e)^4\ (2e)^4\ (8a_1)^2\ (3e)^4\ (4e)^4\ (5e)^4\ (1e^*)^0\ (1a_1{}^*)^0\ (2e^*)^0$.

HC_7N					CH_3C_7N				
State	Dominant orbital excitation	Vertical energy (λ)	f [a]	*0-0* transition energy (λ)	State	Dominant orbital excitation	Vertical energy (λ)	f [a]	*0-0* transition energy [c] (λ)
$A\ ^1\Sigma^-$	$4\pi\rightarrow1\pi^*$	3.29 (377)	0	2.84 (437)	$A\ ^1A_2$	$5e\rightarrow1e^*$	3.23 (384)	0	2.75 (451)
$B\ ^1\Delta$	$4\pi\rightarrow1\pi^*$	3.40 (365)	0	2.96 (419)	$B\ ^1E$	$5e\rightarrow1e^*$	3.34 (371)	0	2.9 (428)
$C\ ^1\Sigma^-$	$3\pi\rightarrow1\pi^*$	5.10 (243)	0	4.79 (259)	$C\ ^1A_2$	$4e\rightarrow1e^*$	5.05 (246)	0	4.73 (262)
$D\ ^1\Delta$	$3\pi\rightarrow1\pi^*$	5.27 (235)	0	4.98 (249)	$D\ ^1E$	$4e\rightarrow1e^*$	5.22 (238)	0.0001	4.92 (252)
$E\ ^1\Sigma^+$	$4\pi\rightarrow1\pi^*$	5.84 (212)	2.9	5.63 (220)	$E\ ^1A_1$	$5e\rightarrow1e^*$	5.61 (221)	2.9	5.40 (230)
					$F\ ^1E$	$5e\rightarrow1a_1{}^*$	6.18 (201)	0	
					$G\ ^1A_2$	$5e\rightarrow2e^*$	6.2 (200)	0	
$F\ ^1\Sigma^+$	$3\pi\rightarrow1\pi^*$	6.23 (199)	0.78	5.86 (212)	$H\ ^1A_1$	$4e\rightarrow1e^*$	6.25 (198)	1.2	
					$I\ ^1E$	$5e\rightarrow2e^*$	6.25 (198)	0.0002	
$a\ ^3\Sigma^+$	$4\pi\rightarrow1\pi^*$			2.25 (551)	$a\ ^3A'$ [b]	$5e\rightarrow1e^*$			2.23 (556)

[a]Value of zero indicates $f < 5 \cdot 10^{-5}$. [b]C_s geometry uncertain; C_{3v} (leading to A_1 triplet state symmetry) also possible, albeit less likely. [c]Derivation of missing *0-0* energy entries was impeded by numerical problems (inherent to the applied method).

The nature of $E - X$ transitions is in both molecules similar to that of $A - X$ or $B - X$, in the sense that they all involve mainly the HOMO–LUMO excitations. $A - X$ transitions (either Σ^-–Σ^+ or A_2–A_1) are formally not allowed for both molecules, while $B - X$, forbidden for HC_7N (Δ–Σ) and formally allowed for CH_3C_7N (E–A_1), is in fact effectively forbidden also for this latter molecule. One may nevertheless expect to see the $B - X$ absorption of CH_3C_7N due to the

Herzberg–Teller vibronic coupling of electronic excitation with one of the vibrational bending modes, a phenomenon reported for shorter cyano-[22,54,55] and methylcyanopolyacetylenes[24,29]. The Herzberg-Teller effect was supposed to occur if the electronic transition dipole moment significantly increased from its equilibrium value after distorting a molecule along a particular normal vibrational coordinate. In our simulations performed for HC_7N (see *Computational details*), only the ν_{10} mode coordinate produced such an effect. $A^1\Pi - X^1\Sigma^+$ bands are expected to have very low intensity; merely traces of that system were observed for CH_3C_5N[29] and for HC_5N.[55]

Molecular geometries for the states $X^1\Sigma^+$, $B^1\Sigma^+$, $E^1\Sigma^+$, and $a^3\Pi$, involved in the experimentally explored electronic transitions of HC_7N and CH_3C_7N, are depicted in Figure 1 (predictions for the other states of Table 1 can be found in Figure S1). Ground-state HC_7N and CH_3C_7N possess conjugated carbon-nitrogen backbones of closely similar geometries. Noteworthy, heavy-atom skeleton changes accompanying $B^1\Sigma^+ - X^1\Sigma^+$ transition are, for both molecules, almost identical to those of $a^3\Pi - X^1\Sigma^+$. One may therefore expect the main vibronic progressions in $B^1\Sigma^+ - X^1\Sigma^+$ absorption and in phosphorescence spectra to be shaped by vibrational modes of similar nature, just as observed for the HC_5N/CH_3C_5N pair.[29] Conversely, the geometry change occurring upon the transition from $X^1\Sigma^+$ to $E^1\Sigma^+$ is much different from those characterizing $a^3\Pi - X^1\Sigma^+$ or $B^1\Sigma^+ - X^1\Sigma^+$.

It is worth noting that our optimizations of CH_3C_7N geometry formally indicate, for the $a^3\Pi$ state, the point group C_s, rather than C_{3v}; the effect comes primarily from a small lowering of the CH_3 group symmetry (see Figure 1). We currently cannot conclude whether this deviation from C_{3v} is or is not a numerical artifact. However, even if it were real, it would have not, (considering its magnitude) show up in the low-resolution spectra produced in this study.

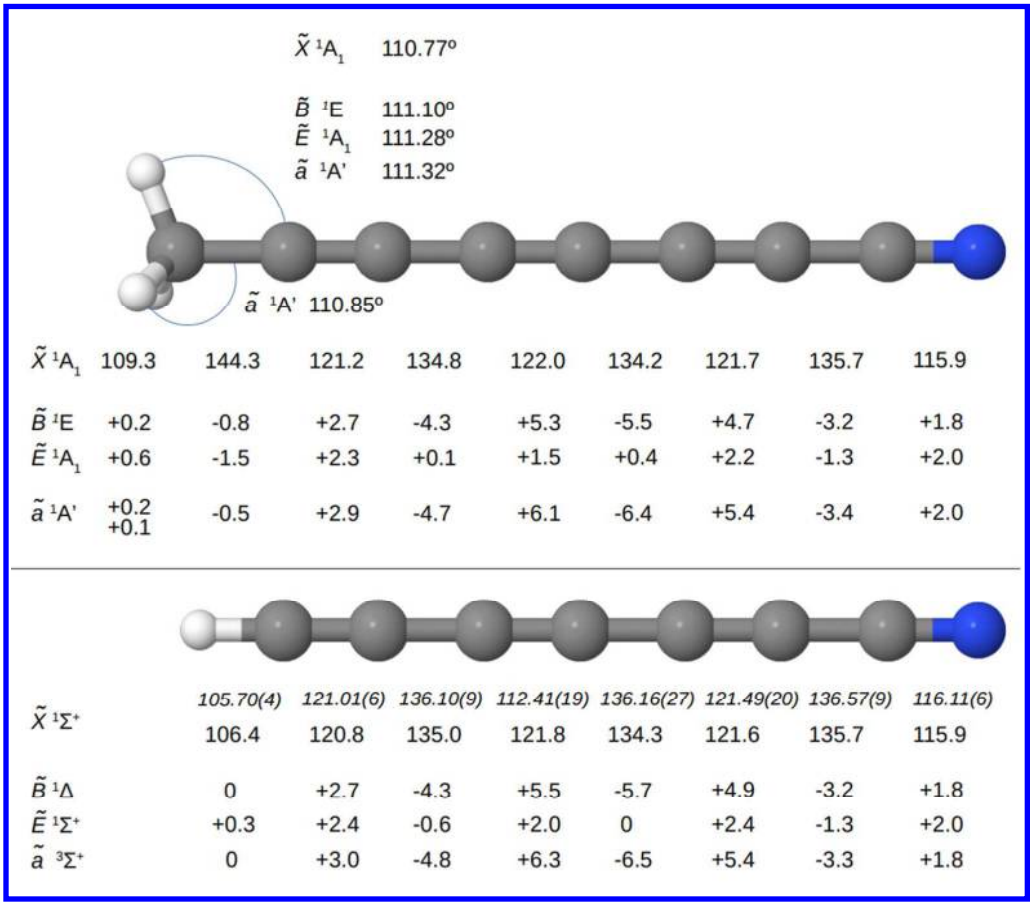

Figure 1. CH_3C_7N and HC_7N geometry in the ground and excited electronic states, as derived at the B3PW91/aug-cc-pVTZ level of theory. Experimental parameters of HC_7N (in italics) are cited after McCarthy et al., Ref. 56. Interatomic distances in pm. Values listed for the excited electronic states are relative, calculated with respect to $\tilde{X}$. For higher electronic states, see Figure S1 of Supporting Information.

Table 2. Harmonic wavenumbers of vibrational modes ($\tilde{\nu}$; scaled by 0.96) for the ground and selected excited electronic states of HC_7N and CH_3C_7N, together with ground-state infrared intensities (*IR*) and Raman activities (*R*), as derived at the B3PW91/aug-cc-pVTZ level of theory. Mode symmetry descriptions refer strictly to the ground electronic states. See Tables S1 and S2 of the Supporting Information for the visualization of vibrations.

	HC_7N						CH_3C_7N				
Mode	$\tilde{X}$			$\tilde{B}$	$\tilde{E}$	Mode	$\tilde{X}$			$\tilde{B}$	$\tilde{E}$
	$\tilde{\nu}$ cm^{-1}	*IR* km/mol	*R* Å^4/amu	$\tilde{\nu}$ cm^{-1}	$\tilde{\nu}$ cm^{-1}		$\tilde{\nu}$ cm^{-1}	*IR* km/mol	*R* Å^4/amu	$\tilde{\nu}$ cm^{-1}	$\tilde{\nu}$ cm^{-1}
	σ symmetry						a_1 symmetry				
ν_1	3324	156	18	3316	3290						
						ν_1	2910	8.9	1223	2882	2841
ν_2	2253	88	1600	2117	2172	ν_2	2260	7.9	100	2114	2180
ν_3	2197	133	9800	2033	2073	ν_3	2208	410	10000	2038	2132
ν_4	2154	5	1600	1907	1949	ν_4	2187	290	8500	1968	1969
ν_5	2049	0	445	1819	1855	ν_5	2093	0.014	7.3	1848	1917
						ν_6	1364	1.3	89	1460	1323
						ν_7	1333	7.7	78	1332	1295
ν_6	1295	0	24	1393	1252	ν_8	1066	0.7	13	1082	1061
ν_7	902	3	0.41	926	884	ν_9	758	6.7	0.88	767	745
ν_8	464	0	2.7	477	456	ν_{10}	402	1.0	1.9	412	395
π symmetry						e symmetry					
						ν_{11}	2976	1.9	370	2892	2894
						ν_{12}	1398	21	27	1384	1352
						ν_{13}	991	4.3	12	1022	953
ν_9	643	80	14	522 [a]	541						
ν_{10}	602	1	57	553 [a]	517	ν_{14}	574	2.3	33	523	490
ν_{11}	523	2	0.001	483	434	ν_{15}	518	4.4	0.092	476	437
ν_{12}	461	10	4.0	434	412	ν_{16}	463	2.2	5.3	419	417
						ν_{17}	340	6.4	4.7	289	212
ν_{13}	287	0	1.7	290	211	ν_{18}	226	0.036	0.28	172	193
ν_{14}	162	13	1.0	153	71	ν_{19}	124	12	0.27	92	57
ν_{15}	61	0	1.8	60	41	ν_{20}	47	0.0010	0.072	43	39

[a]Reversed order; ν_9 corresponds to the H-C vibration.

Vibrational frequencies computed for the selected electronic states (of interest to the analysis of IR spectra or of vibronic features) are collected in Table 2. The only available IR absorption spectrum of CH_3C_7N was measured over 60 years ago by Bohlmann and Mannhardt[31] for a CCl_4 solution; digitization of the published figure points to band maxima at approximately 2290, 2240, 2210, and 2190 cm^{-1}. Our DFT results predict two very intense IR transitions, ν_3 and ν_4, at,

respectively 2208 cm^{-1} and 2187 cm^{-1}, i.e. matching the two of those observed. Other bands are expected to be much weaker. The 2240 and 2290 cm^{-1} bands observed in CCl_4 could correspond to the ν_2 band, possibly split by an anharmonic interaction (such interactions, involving triple-bond stretching modes, were recognized[28] for CH_3C_5N). In our study[37] of the photochemically generated non-methylated analogue, HC_7N, the IR absorption spectroscopy of solid Ar-isolated substance revealed traces of ν_3 (2202.0 cm^{-1}) and ν_1 (3323.1 cm^{-1}) bands, close to the theoretically predicted values. However, in the present experiments, aimed at CH_3C_7N, no IR absorption of this compound could be detected, and the identification was based solely on the analysis of electronic luminescence, just as in our recent study on UV-assisted synthesis of HC_9N from smaller chain precursor molecules.

B. Dispersed phosphorescence

In line with our previous studies, the aim here was to detect CH_3C_7N by means of its phosphorescence, predicted to appear (Table 1) in the vicinity of the $a \rightarrow X$ bands of HC_7N. However, the use of HC_5N as one of the precursors implied the observation of its own intense phosphorescence, partly coinciding with anticipated CH_3C_7N/HC_7N emissions. Consequently, all detected HC_5N bands had to be thoroughly assigned. A listing of these, appending our former report,[55] is available as the Supporting Information, Table S3 and Figures S2 and S3.

Luminescence from photoproducts generated in a $Kr/CH_3C_2H/HC_5N$ matrix was detected especially in spectral windows around 19 700 cm^{-1} (508 nm, 2.44 eV; see Figure 2) and 17 500 cm^{-1} (571 nm, 2.17 eV), corresponding to the most intense phosphorescence bands of HC_7N.[37] An emission/excitation graph (for the first of the above-mentioned spectral ranges) is shown in

Figure 2a. Two closely spaced emission bands are clearly discerned there; their individual excitation patterns indicate the presence of two disparate products. Another strong doublet, with components similarly spaced by ~60 cm^{-1}, appeared in the 17 500 cm^{-1} region. The stronger component shown in Figure 2b corresponds to a lower wavenumber, and is coincident with an already known[37,57] HC_7N emission band. It further gains intensity when excited at 46 430 cm^{-1} (215.4 nm, 5.76 eV; see Figure 2a), in agreement with an excitation maximum previously observed for HC_7N. The other band, with a different excitation spectrum (maximal signal observed upon excitation at 43 150 cm^{-1}, 231.7 nm, 5.35 eV), can be assigned to CH_3C_7N. Indeed, theory predicted (Table 1) for HC_7N almost identical phosphorescence origin energy as for its methylated analogue. It should be noted that the applied computational method is not precise enough to rely on the exact magnitude of the difference between these two values.

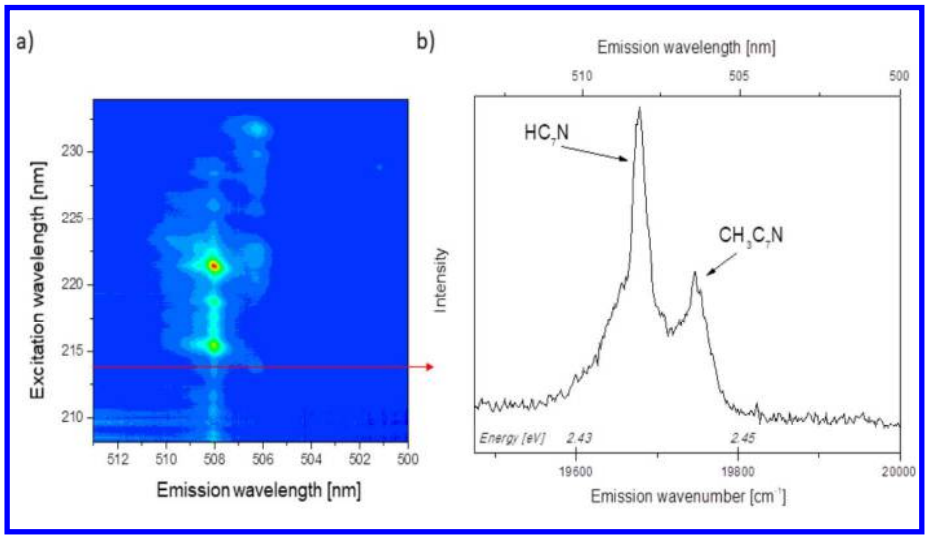

Figure 2. The excitation-emission map of a photolyzed (193 nm) Kr/CH_3C_2H/HC_5N (1000/1/1) matrix showing the spectral features of HC_7N and CH_3C_7N phosphorescence (a). Red color represents the highest and deep blue the lowest phosphorescence intensity. Spectrum (b) corresponds to cross-sectioning the map along the red line, i.e. to phosphorescence excited at 213.5 nm (46 840 cm^{-1}).

The upper trace of Figure 3 presents HC_7N phosphorescence for a photolyzed $Kr/CH_3C_2H/HC_5N$ matrix, excited at a maximum of UV absorption (215.4 nm, Figure 2). The respective wavenumbers of vibronic bands are listed in Table 3, together with the values measured in previous $Ar/HC_5N/C_2H_2$ [37] and $Kr/HC_5N/C_2H_2$ [57] experiments; an additional, fairly weak band, identified as 3_3^0, has been presently detected.

Table 3. HC_7N phosphorescence ($a\ ^3\Sigma^+ \rightarrow X\ ^1\Sigma^+$) bands, as measured in cryogenic matrices. Wavenumber ($\tilde{\nu}$) values in cm^{-1}. Relative wavenumbers ($\Delta\tilde{\nu}$) calculated with respect to the preceding element of the vibronic progression.

Ar (Ref. 37)		Kr (Ref. 57)		Kr (this work)		
$\tilde{\nu}$	$\Delta\tilde{\nu}$	$\tilde{\nu}$	$\Delta\tilde{\nu}$	$\tilde{\nu}$	$\Delta\tilde{\nu}$	Assignment
19764	-	19700	-	19690	-	0_0^0
17565	2199	17500	2200	17490	2200	3_1^0
15378	2187	15310	2190	15310	2180	3_2^0
				13140 [a]	2170 [a]	3_3^0

[a] ±20 cm^{-1}; the band is weak and broad.

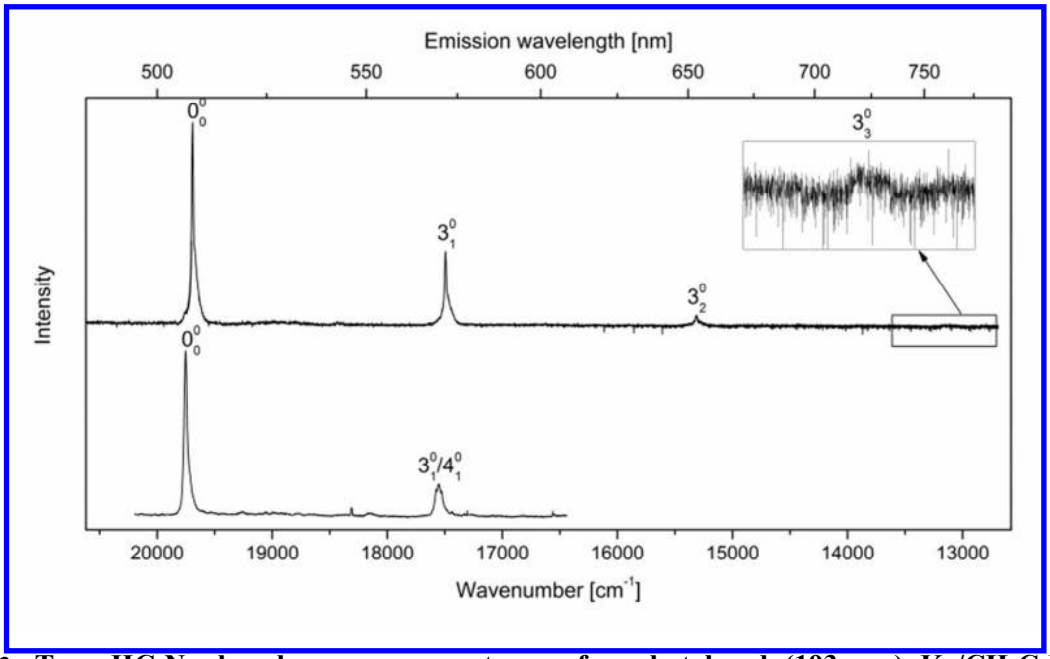

Figure 3. Top: HC_7N phosphorescence spectrum of a photolysed (193 nm) $Kr/CH_3C_2H/HC_5N$ (1000/2/1) matrix excited at 46 430 cm^{-1} (5.76 eV, 215.4 nm). Bottom: CH_3C_7N phosphorescence of a photolyzed (193 nm) $Kr/CH_3C_2H/HC_5N$ (1000/2/1) matrix excited at 43 150 cm^{-1} (5.35 eV, 231.7 nm).

Just as indicated by Figure 2a, the excitation at 231.7 nm led preferably to the phosphorescence of CH_3C_7N (lower curve of Figure 3), with prominent 19 750 cm^{-1} and 17 550 cm^{-1} bands, very similar to that of HC_7N. Of note, the observed CH_3C_7N phosphorescence was less intense than that of HC_7N, preventing the detection of lower frequency features. The position (corresponding to 2.45 eV) of the most intense of the said bands matches reasonably well (the same quality of agreement as for HC_7N) with what is expected (2.23 eV, Table 1) for the vibrationless origin of the $a\,^3A' \rightarrow X\,^1A_1$ system. The bands are 2200 cm^{-1} apart, in acceptable agreement with the present predictions (see Table 2) for either ν_4 or ν_3 X-state frequencies. Using the HC_7N case as a guide, preference could possibly be given to the pseudosymmetric mode ν_4 (2187 cm^{-1}; see Table S2 in Supporting Information for the visualization). Similar reasoning was used[29] in the analysis of the CH_3C_5N spectrum, based on its resemblance to that of HC_5N. However, constancy of HC_7N/CH_3C_7N "splitting" observed in the consecutive elements of the vibronic progression suggests that the vibrational quantum governing the progression of CH_3C_7N is very close to 2200 cm^{-1}, i.e. to the value found for the analogous progression of HC_7N. This points to the mode ν_3 (2208 cm^{-1}) rather than ν_4. Additionally, ν_3 shows the highest Raman activity, and the stretchings of such a character have already been shown to shape the main vibronic progressions of cyanopolyacetylenic molecules.[40,57,58] Broadness of the 17 550 cm^{-1} band may in fact suggest the presence of overlapping ν_3 and ν_4 progressions (the Raman activity of ν_4 is also high).

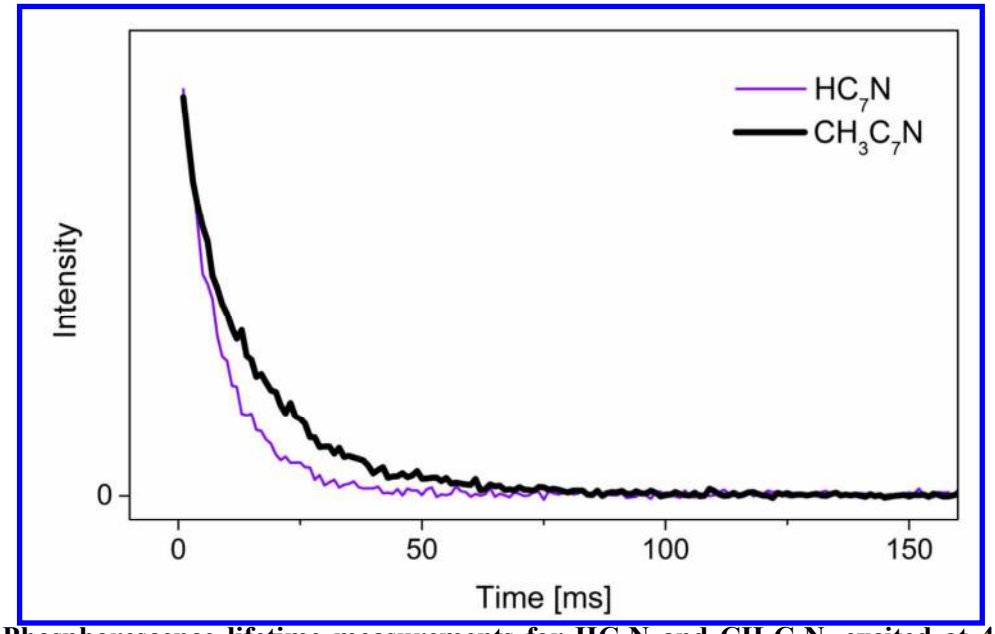

Figure 4. Phosphorescence lifetime measurements for HC_7N and CH_3C_7N, excited at 46 430 cm^{-1} (215.4) nm and 43 150 cm^{-1} (231.7 nm), respectively.

HC_7N and CH_3C_7N emission decays were registered, as demonstrated in Figure 4. The band assigned to the origin of HC_7N phosphorescence showed a mono-exponential decay with $\tau = (8 \pm 0.5)$ ms. This Kr-matrix value is by far smaller than $\tau = (34 \pm 1.5)$ ms reported[37] for solid Ar. The band marking the origin of CH_3C_7N emission was decaying with $\tau = (15 \pm 1)$ ms.

Table 4. Phosphorescence lifetime (ms) for solid Kr-isolated cyanopolyacetylenes and methylcyanopolyacetylenes.

HC_nN	τ	CH_3C_nN	τ
HC_5N [a]	40	CH_3C_5N [b]	150
HC_7N	8	CH_3C_7N	15
HC_9N [c]	3.9		

[a]After Ref. 57. [b]After Ref. 29. [c]After Ref. 39.

These data, together with those reported for other $H(C{\equiv}C)_nCN$ and $CH_3(C{\equiv}C)_nCN$ molecules isolated in solid Kr, are collected in Table 4. Within each of these series, there is a pronounced decrease of lifetime as the length of a polyacetylenic backbone increases. Such a regularity most

likely originates in the diminishing singlet-triplet gap and in the increasing number of chain-deforming vibrational modes; both factors may enhance non-radiative relaxation channels. H-capped cyanopolyacetylenes are characterized by shorter phosphorescence lifetimes than their methylated derivatives. It remains an open question whether this effect is of an intramolecular or of an environmental nature. One may speculate that matrix trapping sites occupied by $C_{\infty v}$ molecules are tighter than those available to their C_{3v} analogues (less Kr atoms need to be removed from an fcc lattice to accommodate an H-capped than a CH_3-capped molecule), and hence the interaction of $C_{\infty v}$ species with lattice phonons is stronger, promoting the non-radiative electronic relaxation.

C. Singlet excited electronic states

Resemblance of the chromophores of HC_7N and CH_3C_7N is illustrated by the predicted geometries (Figure 1). It is also reflected in the corresponding DFT-derived electronic transition energies (Table 1), characterized by similarities already seen within the pairs of methyl- and hydrogen-capped cyanopolyacetylenes CH_3C_3N/HC_3N[22,24,54] or CH_3C_5N/HC_5N[29]. Singlet-singlet electronic absorption features of CH_3C_7N and HC_7N (accessed here by means of phosphorescence excitation) were therefore expected to partially overlap.

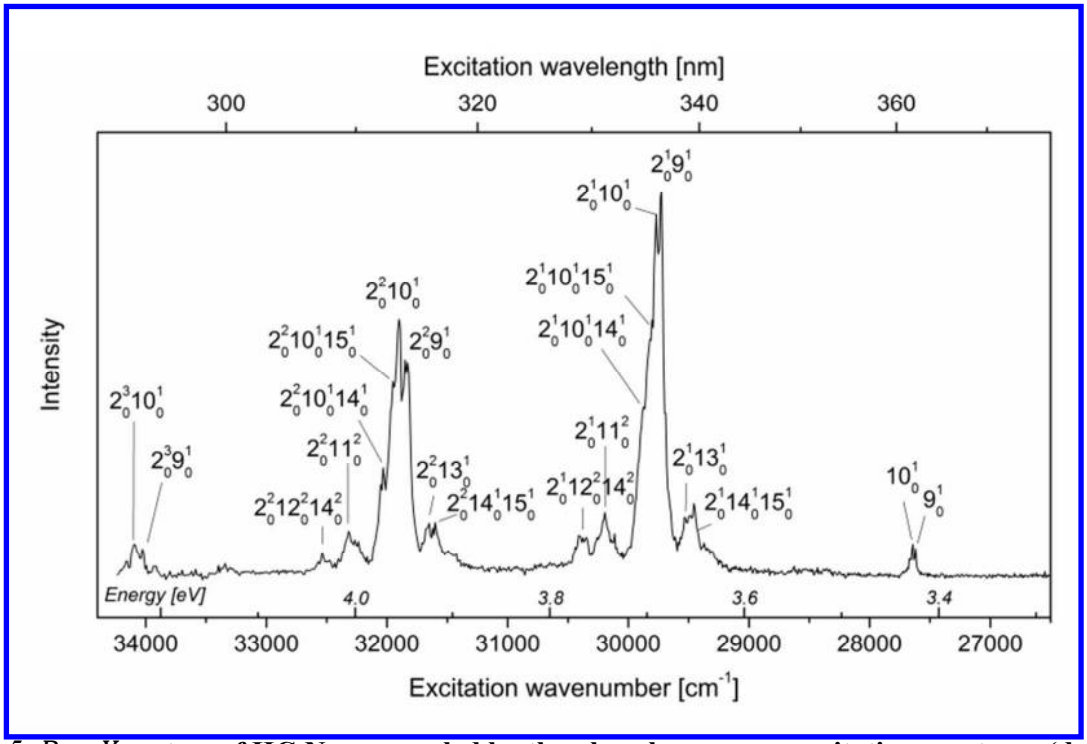

Figure 5. $\tilde{B} - \tilde{X}$ system of HC_7N, as revealed by the phosphorescence excitation spectrum (detection at the 3^1_0 band; 17 500 cm^{-1}) of a photolyzed (193 nm) Kr/C_4H_2/HC_5N (1000/1/1) matrix. Wavelength-dependent laser intensity variations might distort the phosphorescence intensity pattern. Wavenumbers of tentatively identified bands are listed in Table 5.

A part of the $\tilde{B}\,^1\Delta - \tilde{X}\,^1\Sigma^+$ system of HC_7N is presented in Figure 5. As mentioned in the *Theoretical predictions* subsection, the corresponding "*0-0*" feature (system origin) cannot show up in UV absorption or luminescence excitation spectra. In spite of that, $\tilde{B}\,^1\Delta - \tilde{X}\,^1\Sigma^+$ transitions can occur by the coupling to π-symmetry vibrations (Herzberg-Teller effect). For the analogous electronic systems of HC_3N [54] and HC_5N,[55] this was shown to happen via the promoting *zig-zag* modes, pointing to a similar function, in HC_7N, of the vibration ν_{10} (predicted *B*-state wavenumber of 553 cm^{-1}). This role of ν_{10} was also indicated by transition dipole moment calculations (see *Theoretical predictions*). However, the main bands of the most prominent vibronic progression, spaced by ~2100 cm^{-1}, are clearly doubled, suggesting the involvement of

yet another promoting π-symmetry mode, tentatively identified here as ν_9 (*B*-state wavenumber prediction: 522 cm^{-1}). Given that the lowest-wavenumber doublet was detected at 27 620/27 640 cm^{-1}, the $\tilde{B} - \tilde{X}$ origin is expected around 27 100 or 27 120 cm^{-1}, i.e. 3.36 eV. Further profiting from analogies with shorter $H(C{\equiv}C)_nCN$ species (which, compared to HC_7N, feature similar molecular distortions upon $\tilde{B} - \tilde{X}$ excitation, similar patterns of the excited electronic states distribution, and show similarities in phosphorescence spectra), the spacing of the main vibronic progression can be attributed to the $\tilde{B}$-state mode ν_2 (predicted wavenumber 2117 cm^{-1}), analogous to the ν_3 stretching of $\tilde{X}$ (see Table S1). Wavenumbers of HC_7N bands identified in Figure 5 are listed in Table 5.

The analogous, low energy region of the CH_3C_7N phosphorescence excitation spectrum showed just two weak bands attributable to the $\tilde{B}\ ^1E - \tilde{X}\ ^1A_1$ system, at 29 330 cm^{-1} (3.64 eV) and 31 400 cm^{-1} (i.e. spaced by the value of 2070 cm^{-1}, characteristic of triple bond stretching frequencies). The known spectra of smaller (i.e. n = 1 or 2) $H(C{\equiv}C)_nCN$ and $CH_3(C{\equiv}C)_nCN$ molecules indicate that the forbiddance of $\tilde{B} - \tilde{X}$ transitions (and hence the lack of vibrationless origin bands), strictly valid for $H(C{\equiv}C)_nCN$ species, is in practice effective also for the methyl-capped derivatives. It should be recalled that theory predicts a shift of approx. 500 cm^{-1} (see Table 1) between the $\tilde{B} - \tilde{X}$ origins of HC_7N and CH_3C_7N. A very similar value of 475 cm^{-1} was experimentally found for this shift in the analogous case of the HC_5N, CH_3C_5N pair of molecules.[29,55] Therefore, the 29 330 cm^{-1} and 31 400 cm^{-1} features can be related to the HC_7N doublets around 29 750 and 31 860 cm^{-1}, respectively. The detected bands are presumably due to the coupling of $\tilde{B} - \tilde{X}$ with a 'zig-zag' distortion of the carbon-nitrogen chain, combined with a chain stretching mode. This suggests the placement of $\tilde{B}\ ^1E - \tilde{X}\ ^1A_1$ origin at approx. 3.32 eV, an estimation coming from the appropriate lowering of the above-mentioned value 29 330 cm^{-1}, by

subtracting from it the frequencies of (i) the stretching that governs the main vibronic progression (measured value: 2070 cm^{-1}) and (ii) the vibronic-coupling mode (most likely the ν_{14} *zig-zag* chain-bending; predicted value: 523 cm^{-1}).

Table 5. Wavenumbers (cm^{-1}) of $\tilde{B}\ ^1\Delta - \tilde{X}\ ^1\Sigma^+$ bands tentatively identified in the phosphorescence excitation spectrum of HC_7N in solid krypton.

$\tilde{\nu}$	Assignment
27 620	9_0^1
27 640	10_0^1
29 460	$2_0^1 14_0^1 15_0^1$
29 520	$2_0^1 13_0^1$
29 730	$2_0^1 9_0^1$
29 770	$2_0^1 10_0^1$
30 190	$2_0^1 11_0^2$
30 390	$2_0^1 12_0^2 14_0^2$
31 600	$2_0^2 14_0^2 15_0^2$
31 670	$2_0^2 13_0^1$
31 840	$2_0^2 9_0^1$
31 900	$2_0^2 10_0^1$
31 950	Site / $2_0^2 10_0^1 15_0^1$
32 030	Site / $2_0^2 10_0^1 14_0^1$
32 320	$2_0^2 11_0^2$
32 540	$2_0^2 12_0^2 14_0^2$
34 030	$2_0^3 9_0^1$
34 090	$2_0^3 10_0^1$

Figure 6 presents the dependence of experimentally found $\tilde{B} - \tilde{X}$ origin wavelength on the molecule chain length, for two homologues series: $H(C{\equiv}C)_nCN$ and $CH_3(C{\equiv}C)_nCN$. Also shown, for comparison, are the corresponding theoretical predictions, separately for vertical and vibrationless transitions. All sets of data follow linear patterns and, for a given *n* value, the wavelengths found for $H(C{\equiv}C)_nCN$ and $CH_3(C{\equiv}C)_nCN$ are very close to one another. Moreover,

experimental values are consistently lower than the theoretically derived ones, with a fortuitous agreement between the wavelengths of experimental vibrationless transitions and of theoretical vertical transitions (as already reported for $H(C{\equiv}C)_nCN$ molecules).[39]

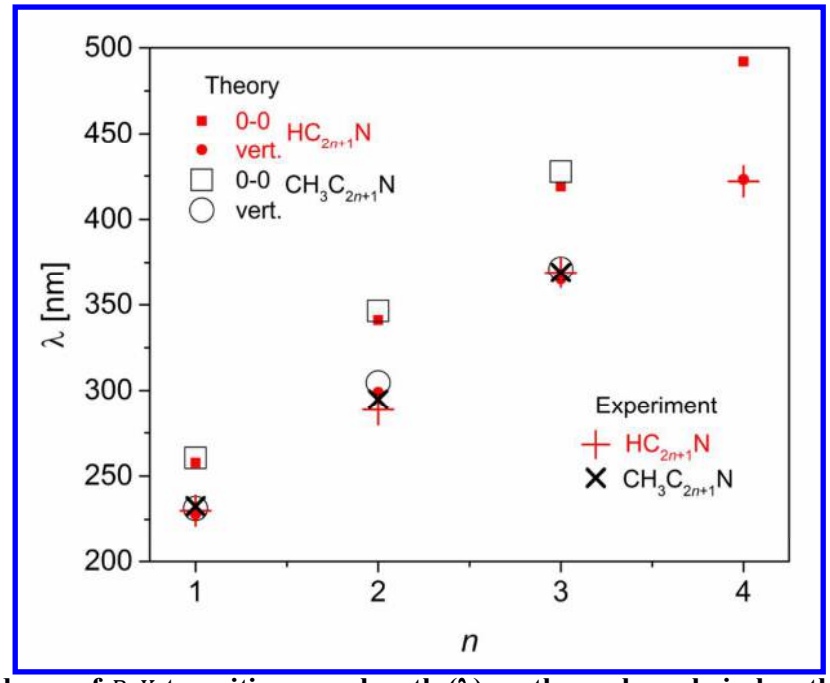

Figure 6. Dependence of $\tilde{B}$-$\tilde{X}$ transition wavelength (λ) on the carbon chain length (n), for $HC_{2n+1}N$ and $CH_3C_{2n+1}N$. Theoretical values are those of this work and Refs. 28, 38. Experimental data correspond to $\tilde{B}$-$\tilde{X}$ origin wavelengths in solid Kr (this work and Refs. 29, 55), with the exception of n = 1: for HC_3N the value found in solid Ar[59] is given (Ar-to-Kr shift being negligible in the scale of the plot), and the CH_3C_3N entry corresponds to the corrected gas-phase value[24] gas-to-Kr shift is estimated as -500 cm^{-1}.

The high-energy region of phosphorescence excitation spectra, above 43 000 cm^{-1}, gave access to fully allowed $\tilde{E} - \tilde{X}$ transitions of HC_7N and CH_3C_7N. Just as predicted (Table 1), the two $\tilde{E} - \tilde{X}$ systems are located very close to one another.

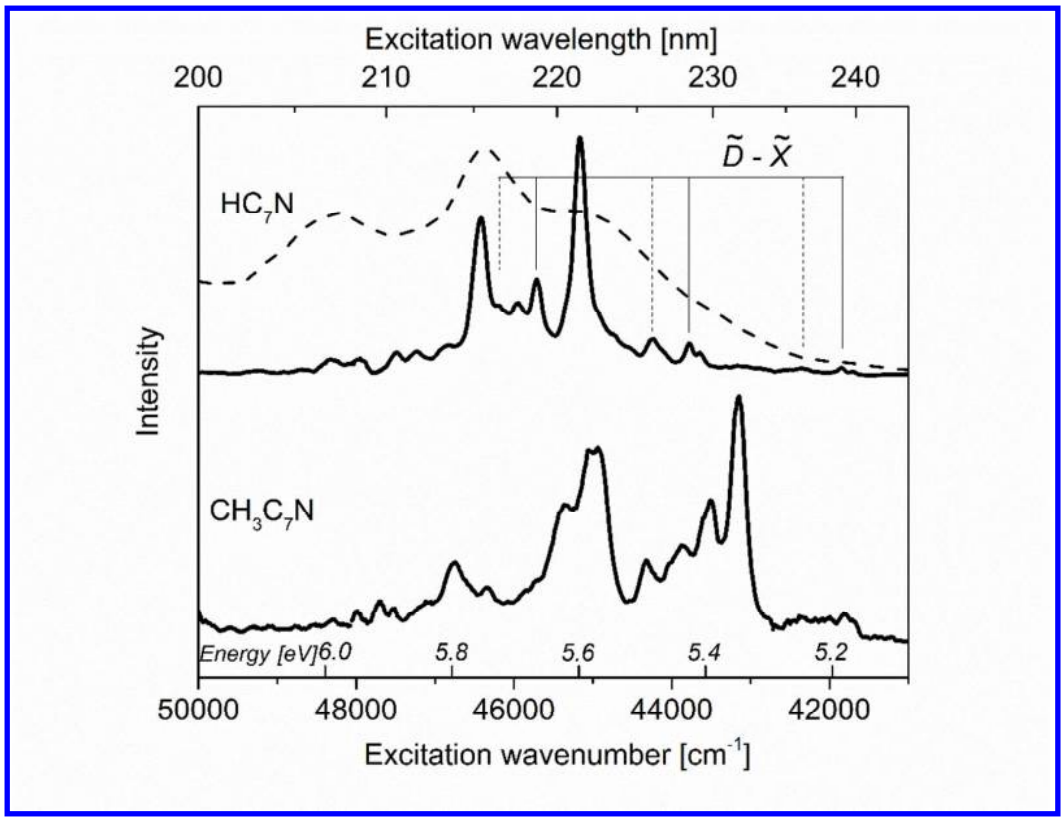

Figure 7. Top: $\tilde{E} - \tilde{X}$ transitions in the excitation spectrum of HC_7N phosphorescence (detection at the *0-0* band, 19 690 cm^{-1}) emitted from a photolyzed (193 nm) $Kr/CH_3C_2H/HC_5N$ (1000/1/1) matrix. Dashed trace (reproduced from Ref. 43) corresponds to the absorption spectrum of HC_7N in acetonitrile. Tentatively identified elements of the $\tilde{D} - \tilde{X}$ vibronic progression are indicated. Bottom: Phosphorescence excitation spectrum (detection at the *0-0* band, 19 750 cm^{-1}) assigned to the $\tilde{E} - \tilde{X}$ electronic system of CH_3C_7N, coming from a $Kr/CH_3C_2H/HC_5N$ (1000/2/1) matrix irradiated at 193 nm. Wavelength-dependent laser intensity variations might distort the phosphorescence intensity patterns.

Figure 7 (bottom) presents the relevant system of bands identified as due to CH_3C_7N. A UV absorption feature reported by Bohlmann[31] for an ether solution of CH_3C_7N (centered at 44 740 cm^{-1}), remains in reasonable agreement with present data. The first strong band of the excitation spectrum is located at 43 150 cm^{-1} (5.35 eV or 231.7 nm), very close to the predicted origin of $\tilde{E}\ ^1A_1 - \tilde{X}\ ^1A_1$ transitions (5.40 eV, see Table 1). Several other bands of this system are

tentatively identified, as proposed in Table 6. The second strong maximum, around 45 000 cm^{-1}, is broad and may correspond to more than one band. Therefore, the main vibronic spacing, given by a distance between the two major spectral features, is not well defined. Its value of ~1800 cm^{-1} is smaller than the closest DFT prediction for $\tilde{E}$ state modes listed in Table 2: ν_5 of 1917 cm^{-1} or ν_4 of 1969 cm^{-1}. It should be noted that the excitation at 43 150 cm^{-1}, which leads to the strongest phosphorescence, was also found to potently destroy the molecule over time (an effect that was not significant for the H-capped analogue). This contributed to a relatively high intensity of detected HC_7N bands compared to those of CH_3C_7N.

Table 6. Vibronic band attributions proposed for the $\tilde{E} - \tilde{X}$ electronic system of CH_3C_7N. Wavenumbers (cm^{-1}) rounded to the nearest 10. Relative wavenumbers give the distance from the vibrationless 0_0^0 band.

$\tilde{\nu}$	$\Delta\tilde{\nu}$	Tentative assignment
43 150	0	0_0^0
43 520	370	10_0^1
43 880 [a]	730	9_0^1 / 10_0^2
44 330	1180	$9_0^1 10_0^1$
45 000 [b]	1850	5_0^1
45 370	2220	$5_0^1 10_0^1$ / 2_0^1
46 350	3200	$5_0^1 6_0^1$ / $2_0^1 8_0^1$
46 770	3620	5_0^2

[a] This broad band is shifted by ~ 2000 cm^{-1} from another broad feature at lower energy, assigned to $\tilde{D} - \tilde{X}$ (see text), it may therefore also belong to the $\tilde{D} - \tilde{X}$ system, rather than to $\tilde{E} - \tilde{X}$.

[b] Broad band, possibly comprising a 44940 / 45070 cm^{-1} doublet, tentatively due to 5_0^1 coupled with 13_0^2.

The top part of Figure 7 shows the analogous region of the phosphorescence excitation spectrum, as measured for HC_7N (qualitatively similar data, for the compound produced in electric discharges through a HC_3N/Kr mixture, were reported by Turowski et al.[40]). The first intense

band, at 45 180 cm^{-1} (221.3 nm), almost matches the theoretical prediction of 5.63 eV (Table 1). As can be seen in Figure 7, a much less resolved UV absorption of HC_7N in acetonitrile, reported in Wakabayashi et al.,[43] appears in the same spectral region. The resemblance of HC_7N and HC_9N excitation spectra, reported by Szczepaniak *et al.*,[39] helps in the assignment of bands. More precisely, at the low energy side, the spectra of both of HC_7N and HC_9N show weak features, most likely due to the $\tilde{D} - \tilde{X}$ system, with a vibronic spacing of ~1930 cm^{-1} (a typical triple bond stretching frequency). The 45 180 cm^{-1} band does not belong to the $\tilde{D} - \tilde{X}$ progressions (marked in Figure 7) and is assigned here to the origin of the $\tilde{E} - \tilde{X}$ system. Table 7 lists tentative identifications of the most intense bands.

As previously mentioned, theoretical predictions pointed to the similarities between the first excited states of HC_7N and CH_3C_7N (Table 1). However, as depicted by Figure 7, the measured patterns of $\tilde{E} - \tilde{X}$ bands differ for the two molecules, and the presence of $\tilde{D} - \tilde{X}$ transitions in the CH_3C_7N spectrum is less obvious (even if possibly manifested with unresolved bands around 42 000 cm^{-1}). Long vibronic progressions are not expected in $\tilde{E} - \tilde{X}$ spectra, considering that the respective electronic excitation is accompanied by little change in molecular geometry. Our tentative band assignments, provided in Tables 6 and 7, do not involve, for the two molecules, the same types of vibrational modes; it is mainly a C-C stretching (ν_6) for HC_7N and a triple bond stretching (ν_5) for CH_3C_7N. No close equivalent to ν_6 of HC_7N does in fact exist for CH_3C_7N (see Tables S1 and S2 of the Supporting Information), what may explain the differences in band patterns observed for these spectra. Moreover, the vibronic pattern of HC_7N spectrum, more difficult to interpret than that found for CH_3C_7N, might result from the energetic proximity of the two allowed electronic systems: $\tilde{E} - \tilde{X}$ and $\tilde{F} - \tilde{X}$. In the case of CH_3C_7N, the separation of $\tilde{E}$

and $H^1\Pi$ states (analogous to $E^2\Pi$ and $F^2\Sigma^+$ of HC_7N) is substantially larger, probably reducing their mutual interaction.

Table 7. Wavenumbers (cm^{-1}) of the most intense bands observed in the $E^2\Pi - X^2\Pi$ region of the HC_7N excitation spectrum. $D^2\Sigma^+ - X^2\Pi$ bands listed in italics. Relative wavenumbers give the distance from the vibrationless (0_0^0) band of the $E^2\Pi - X^2\Pi$ system.

$\tilde{\nu}$	$\Delta\tilde{\nu}$	Tentative assignment
41 720		$D^2\Sigma^+$ (minor band)
41 860		$D^2\Sigma^+$ (main band)
43 660		$D^2\Sigma^+$ (minor band) + ν(triple bond stretch)
43 790		$D^2\Sigma^+$ (main band) + ν(triple bond stretch)
44 250		$D^2\Sigma^+$ (broad band)
45 180	0	0_0^0
45 720		$D^2\Sigma^+$ (main band) + 2ν(triple bond stretch)
45 960	780	$D^2\Sigma^+$ / $E^2\Pi$ [a]
46 210		$D^2\Sigma^+$ (broad band) + ν(triple bond stretch)
46 430	1250	6_0^1
46 840	1660	$6_0^1 8_0^1$
47 230	2050	3_0^1
47 510	2330	6_0^2
47 960	2780	$6_0^2 8_0^1$
48 340	3160	$6_0^2 8_0^2$

[a] An unassigned band belonging either to $E^2\Pi - X^2\Pi$ (possibly perturbed by coupling to a $D^2\Sigma^+ - X^2\Pi$ transition) or to $D^2\Sigma^+ - X^2\Pi$.

D. Chain-coupling mechanisms

Studies on the synthesis of HC_7N and HC_9N in rare gas matrices suggested that the dominant path may consist in the attack of a (cyano)acetylenic radical on the other, intact precursor molecule.[37,39] Consequently, the following scheme may be at work once $C_5N^\bullet$ becomes available:

$$C_5N^\bullet + CH_3C_2H \rightarrow \mathbf{HC_7N} + CH_3^\bullet, \quad (1)$$

$$C_5N^\bullet + CH_3C_2H \rightarrow \mathbf{CH_3C_7N} + H^\bullet. \quad (2)$$

Although the above scheme is aimed at explaining the reactions occurring in cryogenic matrices, not in the interstellar medium, it is nevertheless in accordance with what Cherchneff *et al.* proposed for monocyanopolyacetylene formation in the circumstellar shell IRC +10 216.[60,61]

The propyne photolysis may also take place, and then the reactions of $CH_3C_2^{\bullet}$ could include:

$$CH_3C_2^{\bullet} + HC_5N \rightarrow \mathbf{CH_3C_7N} + H^{\bullet}. \quad (3)$$

Considering that the detection of products relied on phosphorescence, and that the applied excitation laser beam, not harmful to HC_7N, efficiently photolyzed CH_3C_7N, it was not possible to propose even a rough estimation of relative yields for the reaction channels leading to the two discussed triacetylenic molecules. In this context, it is of interest to note, that our introductory experiments with a matrix-isolated, photolysed 1:1 mixture of CH_3C_2H and HC_3N led to approximately equally intense emissions from the two cyanodiacetylenes: CH_3C_5N and HC_5N. In this case, however, both photoproducts were stable during phosphorescence measurements.

The attempted reactions $CH_3C_5N+C_2H_2$ and $CH_3C_3N+C_2H_2$ did not yield any evidence for the elongation of a carbon chain. This suggest that it is easier to detach the methyl group from propyne (Eq. 1) than from a methylcyano(poly)yne molecule.

The discussed processes could possibly occur with a precursor molecule electronically excited rather than converted into a free radical (i.e. the separate dissociation step might not be distinguishable).

CONCLUSIONS

CH_3C_5N and CH_3C_7N molecules were successfully formed from respective smaller (cyano)acetylenic precursors in UV-stimulated cryogenic processes. Phosphorescence of CH_3C_7N, observed here for the first time, was strong enough to uncover the trace amounts of this compound, below the detection level for IR absorption. HC_7N and CH_3C_7N (both products appear simultaneously) turned out to have almost coincident $\tilde{a} - \tilde{X}$ origin wavelengths, as expected for large carbon-nitrogen chain species where the presence or absence of a terminating methyl group does not strongly affect the chromophore. Present studies provide good prospects for using the same approach to synthesize thus far unexplored CH_3C_9N molecule; phosphorescence emissions of the tetraacetylenes HC_9N and CH_3C_9N are however expected to be even more similar than those of their presently studied triacetylenic analogues.

Previous investigations of similar compounds[37,38,40,57,62,63] were indicating the vibrational mode of the highest Raman activity as the one responsible for the leading progression in phosphorescence spectra. This trend seems to be preserved for HC_7N and CH_3C_7N.

The resemblance of HC_7N and CH_3C_7N chromophores is well marked in their singlet-singlet transitions. As usual for the homologous series of chain compounds, the HOMO-LUMO (either $\pi - \pi^*$ or $e - e^*$) energy gap decreases with the molecular length.[64] Two main electronic systems could be distinguished: a fully allowed one and a strictly (for HC_7N) or effectively (for CH_3C_7N) forbidden one. The forbidden $\tilde{B} - \tilde{X}$ transitions ($\Delta - \Sigma$ and $E - A_1$, for HC_7N and CH_3C_7N, respectively) were rendered detectable through coupling with a chain-bending vibration of the C_7N chromophore. This bending, further coupled to a triple-bond stretching mode, promoted the main vibronic progression, recognized in the phosphorescence excitation spectrum.

SUPPORTING INFORMATION

Geometry of HC_7N and CH_3C_7N in several electronic states; visualization of vibrational modes in selected electronic states of HC_7N and CH_3C_7N; phosphorescence spectra and newly observed band assignment for HC_5N.

ACKNOWLEDGMENTS

This project was supported by the Polish National Science Centre, grant no. 2011/03/B/ST4/02763, French-Polish scientific cooperation programs *Partenariat Hubert-Curien Polonium* No. 27752QB (2012-2013), *Polonium* No. 33570RK (2015-2016), and *PICS* (2014-2016). U. Szczepaniak is a beneficiary of the French Government scholarship *Bourse Eiffel*, managed by Campus France, and of the project "Scholarships for PhD students of Podlaskie Voivodeship" – the project is co-financed by European Social Fund, Polish Government and Podlaskie Voivodeship. J.-C. Guillemin acknowledges the support from the Centre National d'Etudes Spatiales (CNES) and the French program Physique et Chimie du Milieu Interstellaire (PCMI) funded by the Conseil National de la Recherche Scientifique (CNRS) and CNES. Thanks are due to Prof. Tomonari Wakabayashi for sharing his data on electronic absorption of HC_7N.

REFERENCES

(1) Turner, B. E. Detection of Interstellar Cyanoacetylene. *Astrophys. J. Lett.* **1971**, *163*, L35.

(2) Mauersberger, R.; Henkel, C.; Sage, L. J. Dense Gas in Nearby Galaxies. III - HC_3N as an Extragalactic Density Probe. *Astron. Astrophys.* **1990**, *236*, 63–68.

(3) Coustenis, A. The Atmospheric Structure of Titan from Voyager to Cassini. *AGU Spring Meet. Abstr.* **2007**, *44*.

(4) Bockelée-Morvan, D.; Lis, D. C.; Wink, J. E.; Despois, D.; Crovisier, J.; Bachiller, R.; Benford, D. J.; Biver, N.; Colom, P.; Davies, J. K.; et al. New Molecules Found in Comet C/1995 O1 (Hale-Bopp). Investigating the Link between Cometary and Interstellar Material. *Astron. Astrophys.* **2000**, *353*, 1101–1114.

(5) Snell, R. L.; Schloerb, F. P.; Young, J. S.; Hjalmarson, A.; Friberg, P. Observations of HC_3N, HC_5N, and HC_7N in Molecular Clouds. *Astrophys. J.* **1981**, *244*, 45–53.

(6) Truong-Bach; Graham, D.; Nguyen-Q-Rieu. HC_9N from the Envelopes of IRC+10216 and CRL:2688. *Astron. Astrophys.* **1993**, *277*, 133.

(7) Broten, N. W.; MacLeod, J. M.; Avery, L. W.; Friberg, P.; Hjalmarson, A.; Hoglund, B.; Irvine, W. M. The Detection of Interstellar Methylcyanoacetylene. *Astrophys. J.* **1984**, *276*, L25.

(8) Belloche, A.; Müller, H. S. P.; Menten, K. M.; Schilke, P.; Comito, C. Complex Organic Molecules in the Interstellar Medium: IRAM 30 M Line Survey of Sagittarius B2(N) and (M). *Astron. Astrophys.* **2013**, *559*, A47.

(9) Snyder, L. E.; Hollis, J. M.; Jewell, P. R.; Lovas, F. J.; Remijan, A. Confirmation of Interstellar Methylcyanodiacetylene (CH_3C_5N). *Astrophys. J.* **2006**, *647* (1), 412.

(10) Quan, D.; Herbst, E. Possible gas-phase syntheses for seven neutral molecules studied recently with the Green Bank Telescope. *Astron. Astrophys.* **2007**, *10*, 474.

(11) Herbst, E.; Leung, C. M. Gas-Phase Production of Complex Hydrocarbons, Cyanopolyynes, and Related Compounds in Dense Interstellar Clouds. *Astrophys. J. Suppl. Ser.* **1989**, *69*, 271.

(12) Markwick, A. J.; Millar, T. J.; Charnley, S. B. On the Abundance Gradients of Organic Molecules along the TMC-1 Ridge. *Astrophys. J.* **2000**, *535* (1), 256.

(13) Kalvāns, J.; Shmeld, I. Subsurface Chemistry of Mantles of Interstellar Dust Grains in Dark Molecular Cores. *Astron. Astrophys.* **2010**, *521*, A37.

(14) Vuitton, V.; Yelle, R. V.; McEwan, M. J. Ion Chemistry and N-Containing Molecules in Titan's Upper Atmosphere. *Icarus* **2007**, *191* (2), 722–742.

(15) Loison, J. C.; Hébrard, E.; Dobrijevic, M.; Hickson, K. M.; Caralp, F.; Hue, V.; Gronoff, G.; Venot, O.; Bénilan, Y. The Neutral Photochemistry of Nitriles, Amines and Imines in the Atmosphere of Titan. *Icarus* **2015**, *247*, 218–247.

(16) Kerisit, N.; Rouxel, C.; Colombel-Rouen, S.; Toupet, L.; Guillemin, J.-C.; Trolez, Y. Synthesis, Chemistry, and Photochemistry of Methylcyanobutadiyne in the Context of Space Science. *J. Org. Chem.* **2016**.

(17) Sheridan, J.; Thomas, L. F. Microwave Spectrum of Methyl-Cyanoacetylene. *Nature* **1954**, *174* (4434), 798–798.

(18) Tubino, R.; Dellepiane, G.; Zerbi, G. Vibrational Spectrum and Vibro□Rotational Analysis of Cyanopropyne. *J. Chem. Phys.* **1969**, *50* (2), 621–627.

(19) Bossis, G. Le Moment Dipolaire et l'absorption en Infrarouge Lointain du Cyanopropyne, Existence d'une Tres Forte Contribution des Dipoles Temporaires Induits. *Mol. Phys.* **1976**, *31* (6), 1897–1908.

(20) Dello Russo, N.; Khanna, R. K. Laboratory Infrared Spectroscopic Studies of Crystalline Nitriles with Relevance to Outer Planetary Systems. *Icarus* **1996**, *123* (2), 366–395.

(21) Khlifi, M.; Raulin, F. Infrared Intensities and Frequencies of 2-Butynenitrile: Application to the Atmosphere of Titan. *Spectrochim. Acta Part Mol. Spectrosc.* **1991**, *47* (2), 171–176.

(22) Bruston, P.; Poncet, H.; Raulin, F.; Cossart-Magos, C.; Courtin, R. UV Spectroscopy of Titan's Atmosphere, Planetary Organic Chemistry, and Prebiological Synthesis: I. Absorption Spectra of Gaseous Propynenitrile and 2-Butynenitrile in the 185- to 250-nm Region. *Icarus* **1989**, *78* (1), 38–53.

(23) Bieri, G.; Heilbronner, E.; Hornung, V.; Kloster-Jensen, E.; Maier, J. P.; Thommen, F.; Niessen, W. von. Electronic States of Substituted Haloacetylene and Cyanoacetylene Radical Cations. *Chem. Phys.* **1979**, *36* (1), 1–14.

(24) Lamarre, N.; Gans, B.; Vieira Mendes, L. A.; Gronowski, M.; Guillemin, J.-C.; De Oliveira, N.; Douin, S.; Chevalier, M.; Crépin, C.; Kołos, R.; et al. Excited Electronic Structure of Methylcyanoacetylene Probed by VUV Fourier-Transform Absorption Spectroscopy. *J. Quant. Spectrosc. Radiat. Transf.* **2016**, *182*, 286–295.

(25) Alexander, A. J.; Kroto, H. W.; Maier, M.; Walton, D. R. M. The Microwave Spectra of Symmetric Top Polyacetylenes. *J. Mol. Spectrosc.* **1978**, *70* (1), 84–94.

(26) Chen, W.; Grabow, J.-U.; Travers, M. J.; Munrow, M. R.; Novick, S. E.; McCarthy, M. C.; Thaddeus, P. Microwave Spectra of the Methylcyanopolyynes $CH_3(CC)_nCN$, n= 2, 3, 4, 5. *J. Mol. Spectrosc.* **1998**, *192* (1), 1–11.

(27) Montero-Campillo, M. M.; Mó, O.; Yáñez, M.; Benidar, A.; Rouxel, C.; Kerisit, N.; Trolez, Y.; Guillemin, J.-C. Gas-Phase Infrared Spectroscopy of Substituted Cyanobutadiynes: Roles of the Bromine Atom and Methyl Group as Substituents. *ChemPhysChem* **2016**, *17* (7), 1018–1024.

(28) Szczepaniak, U.; Turowski, M.; Custer, T.; Gronowski, M.; Kerisit, N.; Trolez, Y.; Kołos, R. Infrared and Raman Spectroscopy of Methylcyanodiacetylene (CH_3C_5N). *ChemPhysChem* **2016**, *17* (19), 3047–3054.

(29) Turowski, M.; Szczepaniak, U.; Custer, T.; Gronowski, M.; Kołos, R. Electronic Spectroscopy of Methylcyanodiacetylene (CH_3C_5N). *ChemPhysChem* **2016**, *17* (24), 4068–4078.

(30) Kerisit, N.; Toupet, L.; Trolez, Y.; Guillemin, J.-C. Methylcyanobutadiyne: Synthesis, X-Ray Structure and Photochemistry; Towards an Explanation of Its Formation in the Interstellar Medium. *Chem. – Eur. J.* **2013**, *19* (52), 17683–17686.

(31) Bohlmann, F.; Mannhardt, H.-J. Polyacetylenverbindungen, XVIII. Mitteil.: Über die Lichtabsorption von Polyin-Carbonsäurenitrilen. *Chem. Ber.* **1956**, *89* (10), 2268–2272.

(32) Thaddeus, P.; McCarthy, M. C.; Travers, M. J.; Gottlieb, C. A.; Chen, W. New Carbon Chains in the Laboratory and in Interstellar Space. *Faraday Discuss.* **1998**, *109*, 121–135.

(33) McCarthy, M. C.; Chen, W.; Travers, M. J.; Thaddeus, P. Microwave Spectra of 11 Polyyne Carbon Chains. *Astrophys. J. Suppl. Ser.* **2000**, *129* (2), 611.

(34) Arnau, A.; Tuñón, I.; Andrés, J.; Silla, E. Theoretical Rotational Constants of MeC_nN Species. *Chem. Phys. Lett.* **1990**, *166* (1), 54–56.

(35) Woon, D. E.; Herbst, E. Quantum Chemical Predictions of the Properties of Known and Postulated Neutral Interstellar Molecules. *Astrophys. J. Suppl. Ser.* **2009**, *185* (2), 273.

(36) Coupeaud, A.; Kołos, R.; Couturier-Tamburelli, I.; Aycard, J. P.; Piétri, N. Photochemical Synthesis of the Cyanodiacetylene HC_5N: A Cryogenic Matrix Experiment. *J. Phys. Chem. A* **2006**, *110* (7), 2371–2377.

(37) Couturier-Tamburelli, I.; Piétri, N.; Crépin, C.; Turowski, M.; Guillemin, J.-C.; Kołos, R. Synthesis and Spectroscopy of Cyanotriacetylene (HC_7N) in Solid Argon. *J. Chem. Phys.* **2014**, *140* (4), 044329.

(38) Crépin, C.; Turowski, M.; Ceponkus, J.; Douin, S.; Boyé-Péronne, S.; Gronowski, M.; Kołos, R. UV-Induced Growth of Cyanopolyyne Chains in Cryogenic Solids. *Phys. Chem. Chem. Phys. PCCP* **2011**, *13* (37), 16780–16785.

(39) Szczepaniak, U.; Crépin, C.; Gronowski, M.; Chevalier, M.; Guillemin, J.-C.; Turowski, Michał; Custer, T.; Kołos, R. Cryogenic Photochemical Synthesis and Electronic Spectroscopy of Cyanotetraacetylene. *J. Phys. Chem. A* **2017**, *121* (39), 7374-7384.

(40) Turowski, M.; Crépin, C.; Douin, S.; Kołos, R. Formation and Spectroscopy of Dicyanotriacetylene (NC_8N) in Solid Kr. *J. Phys. Chem. A* **2014**, *119* (11), 2701-2708.

(41) Fahr, A.; Laufer, A. H. UV-Absorption Spectra of the Radical Transients Generated from the 193-nm Photolysis of Allene, Propyne, and 2-Butyne. *J. Phys. Chem. A* **2005**, *109* (11), 2534–2539.

(42) Alnama, K.; Boyé-Péronne, S.; Douin, S.; Innocenti, F.; O'Reilly, J.; Roche, A.-L.; Shafizadeh, N.; Zuin, L.; Gauyacq, D. Photolysis of Allene and Propyne in the 7–30eV Region Probed by the Visible Fluorescence of Their Fragments. *J. Chem. Phys.* **2007**, *126* (4), 044304.

(43) Wakabayashi, T.; Saikawa, M.; Wada, Y.; Minematsu, T. Isotope Scrambling in the Formation of Cyanopolyynes by Laser Ablation of Carbon Particles in Liquid Acetonitrile. *Carbon* **2012**, *50* (1), 47–56.

(44) Cataldo, F. Monocyanopolyynes from a Carbon Arc in Ammonia: About the Relative Abundance of Polyynes Series Formed in a Carbon Arc and Those Detected in the Circumstellar Shells of AGB Stars. *Int. J. Astrobiol.* **2006**, *5* (01), 37–45.

(45) Cataldo, F. Polyynes and Cyanopolyynes: Their Synthesis with the Carbon Arc Gives the Same Abundances Occurring in Carbon-Rich Stars. *Orig. Life Evol. Biospheres* **2006**, *36* (5–6), 467–475.

(46) Forte, G.; D'Urso, L.; Fazio, E.; Patanè, S.; Neri, F.; Puglisi, O.; Compagnini, G. The Effects of Liquid Environments on the Optical Properties of Linear Carbon Chains Prepared by Laser Ablation Generated Plasmas. *Appl. Surf. Sci.* **2013**, *272*, 76–81.

(47) Trolez, Y.; Guillemin, J.-C. Synthesis and Characterization of 2,4-Pentadiynenitrile—A Key Compound in Space Science. *Angew. Chem. Int. Ed.* **2005**, *44* (44), 7224–7226.

(48) Miller, F. A.; Lemmon, D. H. The Infrared and Raman Spectra of Dicyanodiacetylene, N≡C–C≡C–C≡C–C≡N. *Spectrochim. Acta Part Mol. Spectrosc.* **1967**, *23* (5), 1415–1423.

(49) Frisch, M. J.; Trucks, G. W.; Schlegel, H. B.; Scuseria, G. E.; Robb, M. A.; Cheeseman, J. R.; Scalmani, G.; Barone, V.; Mennucci, B.; Petersson, G. A.; et al. *Gaussian 09*; Gaussian, Inc.: Wallingford, CT, USA, 2009.

(50) Parr, R. G.; Weitao, Y. *Density-Functional Theory of Atoms and Molecules*; Oxford University Press, 1989.

(51) Perdew, J. P.; Burke, K.; Wang, Y. Generalized Gradient Approximation for the Exchange-Correlation Hole of a Many-Electron System. *Phys. Rev. B* **1996**, *54* (23), 16533–16539.

(52) Dunning, T. H. J. Gaussian Basis Sets for Use in Correlated Molecular Calculations. I. The Atoms Boron through Neon and Hydrogen. *J. Chem. Phys.* **1989**, *90* (2), 1007–1023.

(53) Kendall, R. A.; Jr, T. H. D.; Harrison, R. J. Electron Affinities of the First□row Atoms Revisited. Systematic Basis Sets and Wave Functions. *J. Chem. Phys.* **1992**, *96* (9), 6796–6806.

(54) Job, V. A.; King, G. W. The Electronic Spectrum of Cyanoacetylene: Part II. Analysis of the 2300-Å System. *J. Mol. Spectrosc.* **1966**, *19* (1–4), 178–184.

(55) Turowski, M.; Crépin, C.; Gronowski, M.; Guillemin, J.-C.; Coupeaud, A.; Couturier-Tamburelli, I.; Piétri, N.; Kołos, R. Electronic Absorption and Phosphorescence of Cyanodiacetylene. *J. Chem. Phys.* **2010**, *133* (7), 074310.

(56) McCarthy, M. C.; Levine, E. S.; Apponi, A. J.; Thaddeus, P. Experimental Structures of the Carbon Chains HC_7N, HC_9N, and $HC_{11}N$ by Isotopic Substitution. *J. Mol. Spectrosc.* **2000**, *203* (1), 75–81.

(57) Turowski, M. *Niskotemperaturowe Badania Fotochemii i Spektroskopii Cyjanoacetylenów o Znaczeniu Astrofizycznym.* PhD Dissertation, Institute of Physical Chemistry, Polish Academy of Sciences: Warsaw, Poland, 2012.

(58) Turowski, M.; Crépin, C.; Douin, S.; Gronowski, M.; Couturier-Tamburelli, I.; Piétri, N.; Wasiak, A.; Kołos, R. Low Temperature Raman Spectra of Cyanobutadiyne (HC_5N). *Vib. Spectrosc.* **2012**, *62*, 268–272.

(59) Kołos, R., unpublished result, 2017.

(60) Cherchneff, I.; Glassgold, A. E. The Formation of Carbon Chain Molecules in IRC +10216. *Astrophys. J. Lett.* **1993**, *419*, L41.

(61) Cherchneff, I.; Glassgold, A. E.; Mamon, G. A. The Formation of Cyanopolyyne Molecules in IRC + 10216. *Astrophys. J.* **1993**, *410*, 188–201.

(62) Chang, J.-W.; Lee, Y.-P. The C_2N_2 $a^3\Sigma_u^+ \rightarrow X^1\Sigma_g^+$ Chemiluminescence in Matrices. *J. Mol. Struct.* **1987**, *157* (1–3), 155–165.

(63) Turowski, M.; Crépin, C.; Couturier-Tamburelli, I.; Piétri, N.; Kołos, R. Low-Temperature Phosphorescence of Dicyanoacetylene in Rare Gas Solids. *Low Temp. Phys.* **2012**, *38* (8), 723–726.

(64) Connors, R. E.; Roebber, J. L.; Weiss, K. Vacuum Ultraviolet Spectroscopy of Cyanogen and Cyanoacetylenes. *J. Chem. Phys.* **1974**, *60* (12), 5011–5024.

TOC Graphic

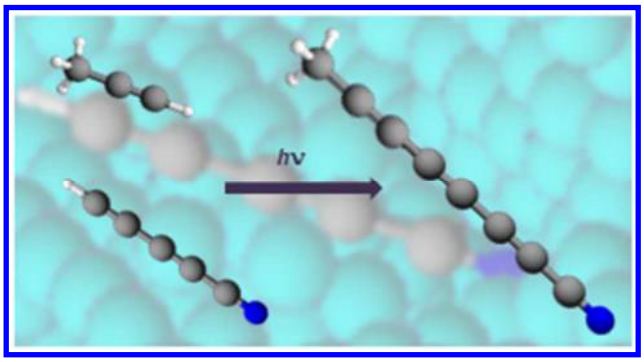

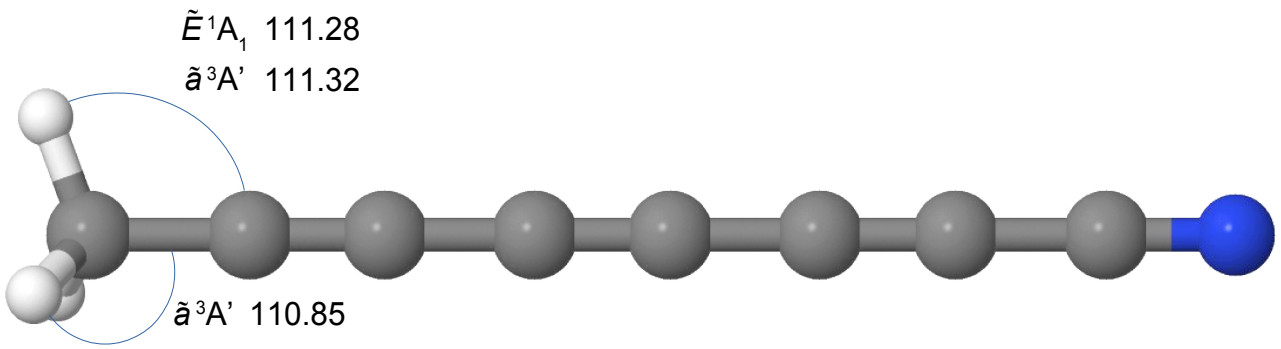

$\tilde{X}\,^1A_1$	109.3	144.3	121.2	134.8	122.0	134.2	121.7	135.7	115.9
$\tilde{B}\,^1E$	+0.2	-0.8	+2.7	-4.3	+5.3	-5.5	+4.7	-3.2	+1.8
$\tilde{E}\,^1A_1$	+0.6	-1.5	+2.3	+0.1	+1.5	+0.4	+2.2	-1.3	+2.0
$\tilde{a}\,^3A'$	+0.2 +0.1	-0.5	+2.9	-4.7	+6.1	-6.4	+5.4	-3.4	+2.0

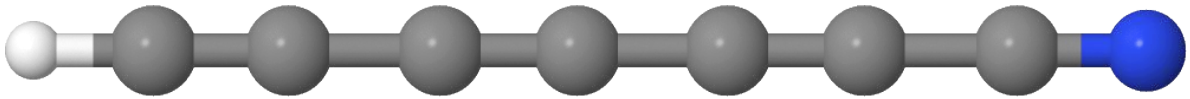

	1.0570(4)	*1.2101(6)*	*1.3610(9)*	*1.1241(19)*	*1.3616(27)*	*1.2149(20)*	*1.3657(9)*	*1.1611(6)*
$\tilde{X}\,^1\Sigma^+$	106.4	120.8	135.0	121.8	134.3	121.6	135.7	115.9
$\tilde{B}\,^1\Delta$	0.0	+2.7	-4.3	+5.5	-5.7	+4.9	-3.2	+1.8
$\tilde{E}\,^1\Sigma^+$	+0.3	+2.4	-0.6	+2.0	0.0	+2.4	-1.3	+2.0
$\tilde{a}\,^3\Sigma^+$	0.0	+3.0	-4.8	+6.3	-6.5	+5.4	-3.3	+1.8

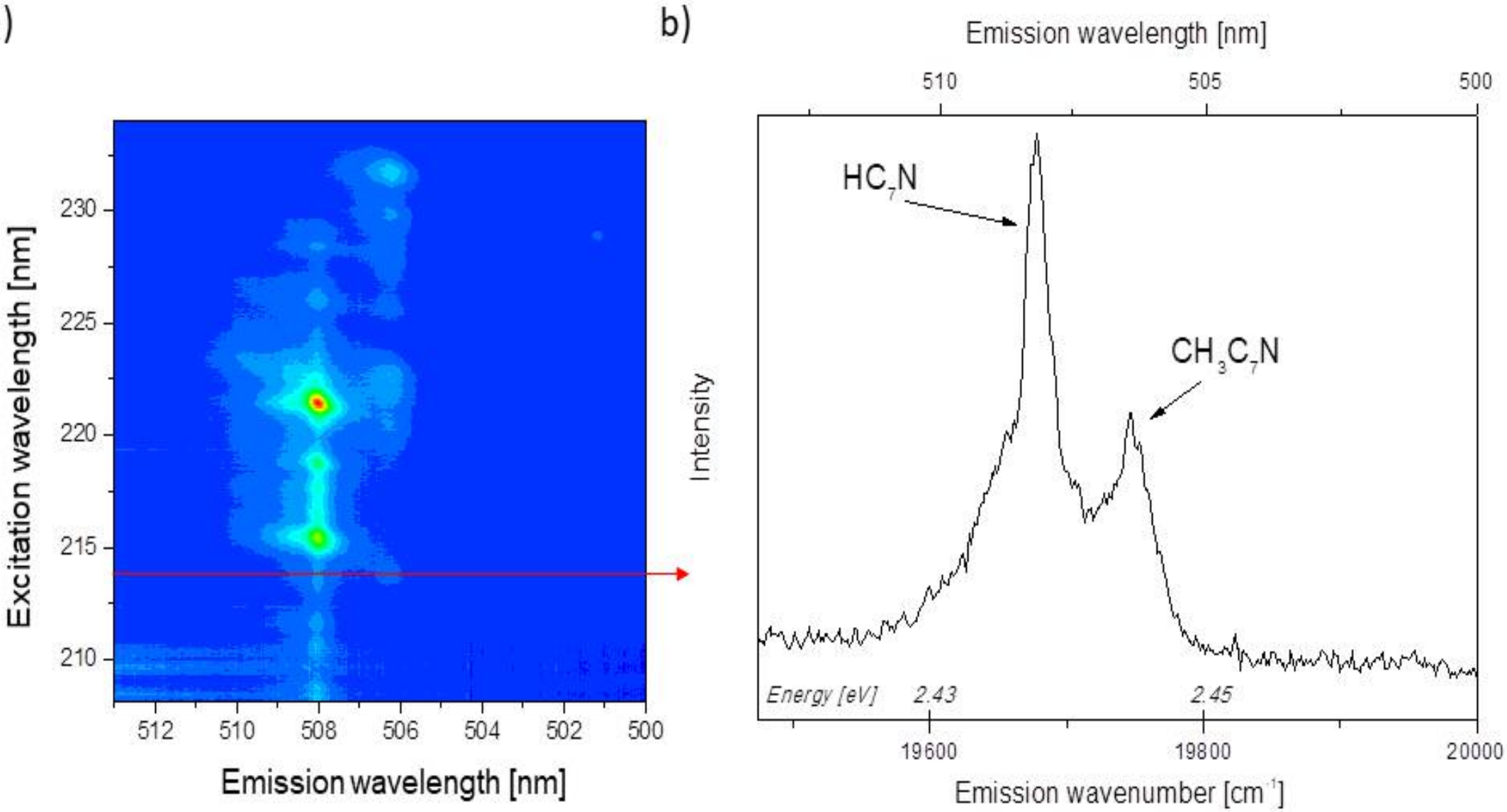
a)
Excitation wavelength [nm]
230
225
220
215
210
512
510
508
506
504
502
500
Emission wavelength [nm]
b)
Emission wavelength [nm]
510
505
500
HC7N
CH3C7N
Intensity
Energy [eV]
2.43
2.45
19600
19800
20000
Emission wavenumber [cm-1]

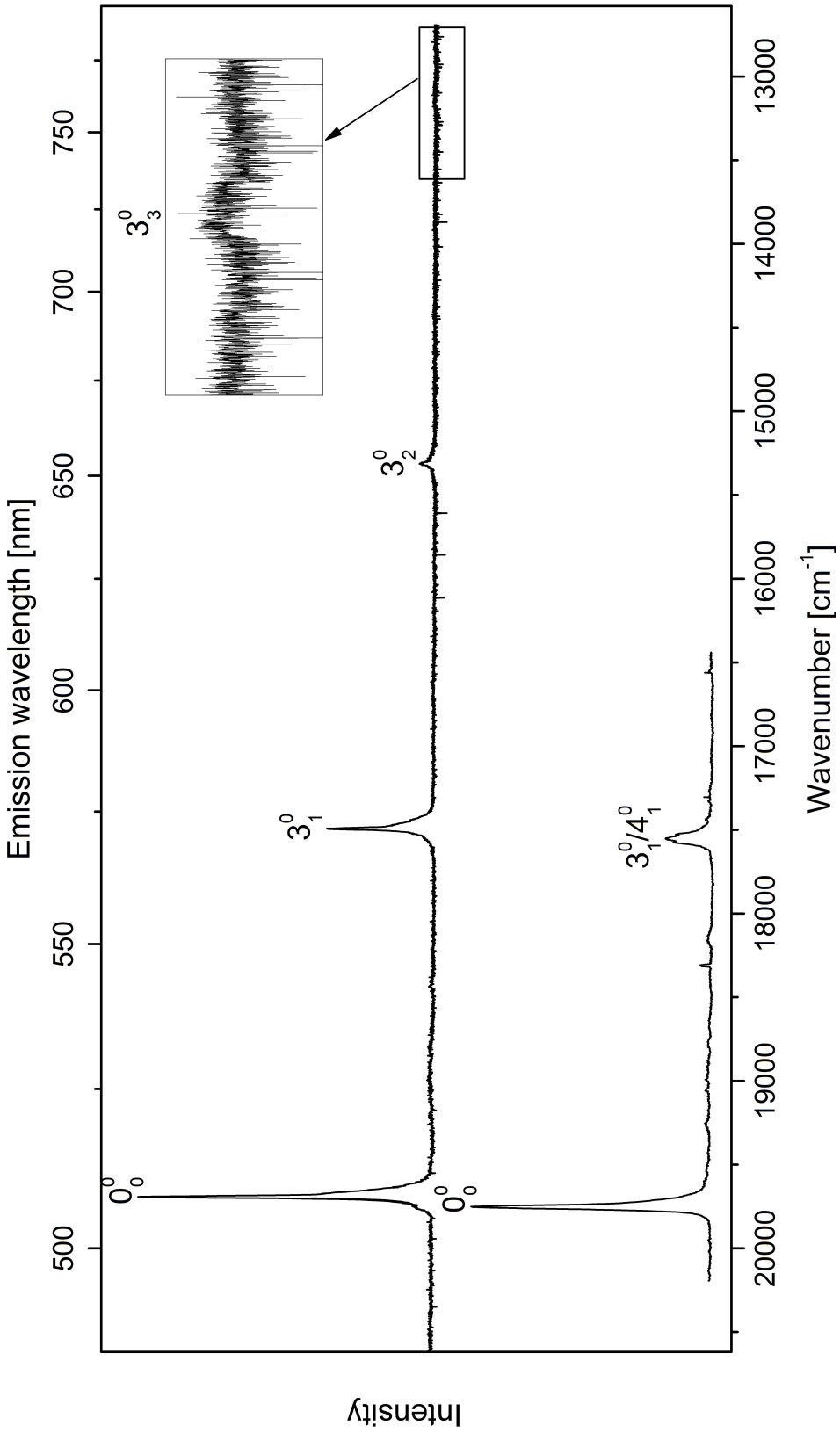
Emission wavelength [nm]
500
550
600
650
700
750
Wavenumber [cm-1]
13000
14000
15000
16000
17000
18000
19000
20000
Intensity
0 0 0
3 1 0
3 2 0
3 3 0
3 1 0 / 4 1 0

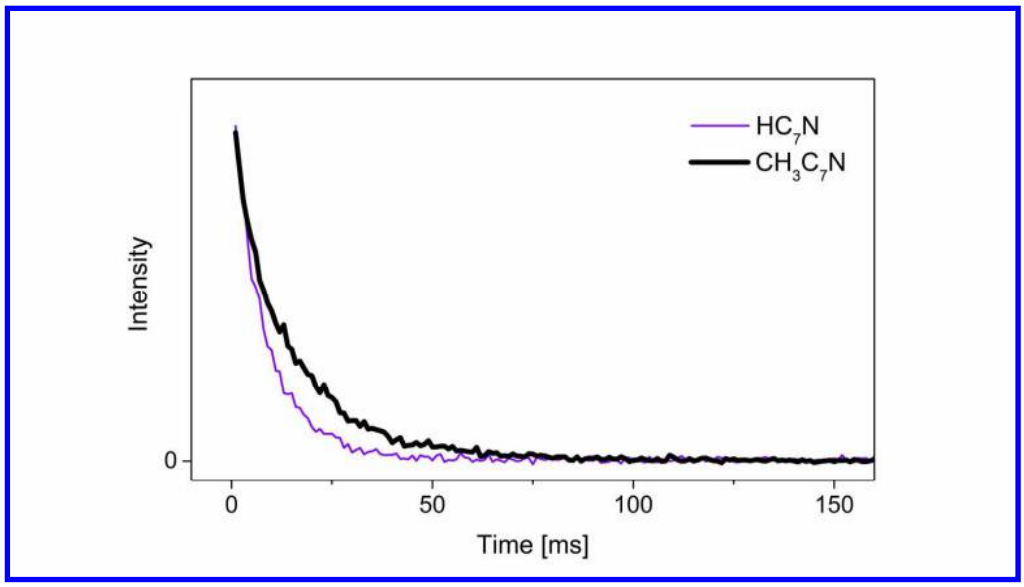

Figure 4.

199x112mm (300 x 300 DPI)

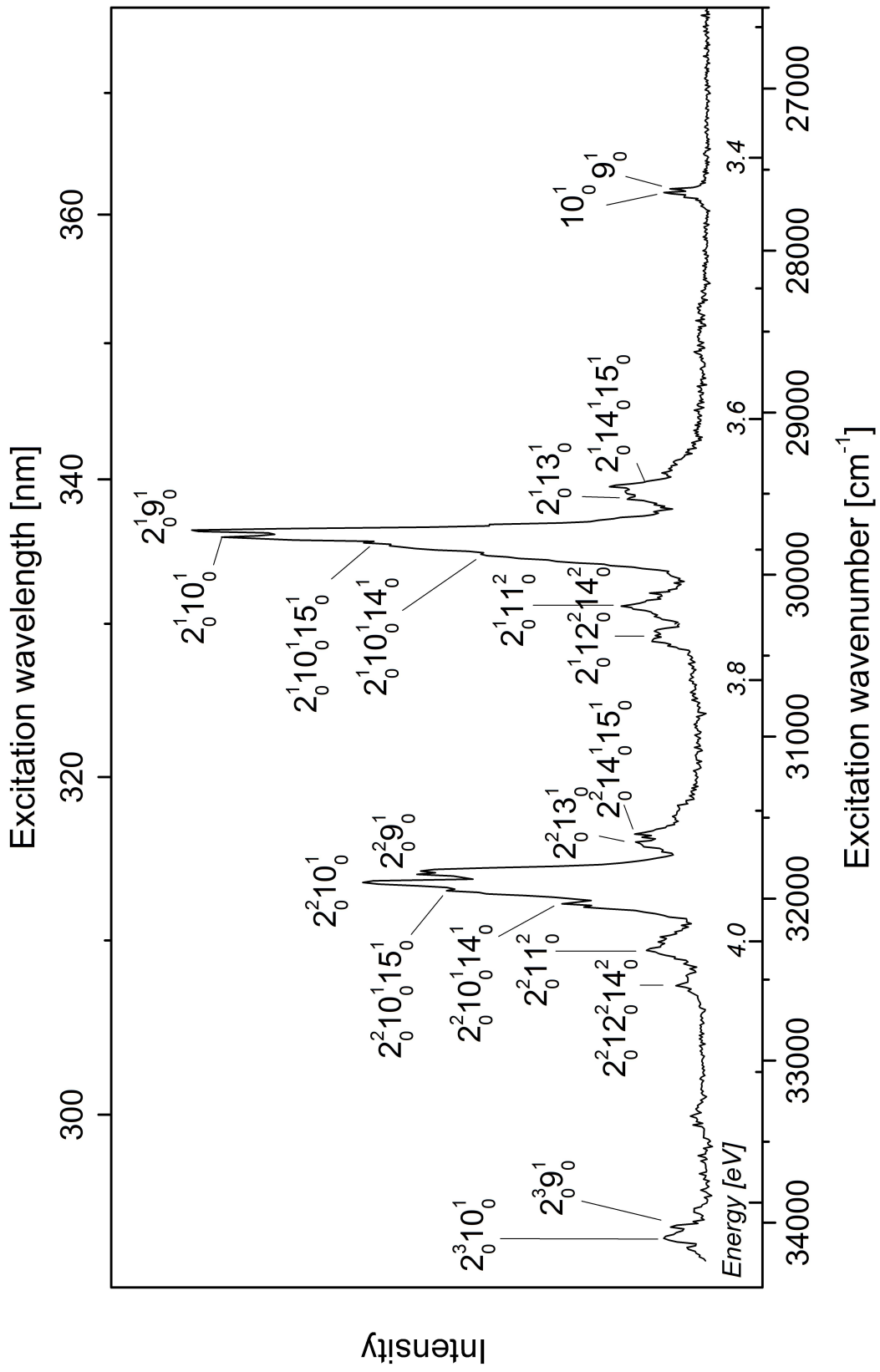
Excitation wavelength [nm]
300
320
340
360
Excitation wavenumber [cm-1]
34000
33000
32000
31000
30000
29000
28000
27000
Energy [eV]
4.0
3.8
3.6
3.4
Intensity
2^3 10^1_0
2^3 9^1_0
2^2 12^2 14^2_0
2^2 10^1 14^1_0
2^2 10^1 15^1_0
2^2 11^2_0
2^2 10^1_0
2^2 13^1_0
2^2 14^1 15^1_0
2^2 9^1_0
2^1 12^2 14^2_0
2^1 10^1 14^1_0
2^1 10^1 15^1_0
2^1 11^2_0
2^1 10^1_0
2^1 13^1_0
2^1 14^1 15^1_0
2^1 9^1_0
10^1_0 9^1_0

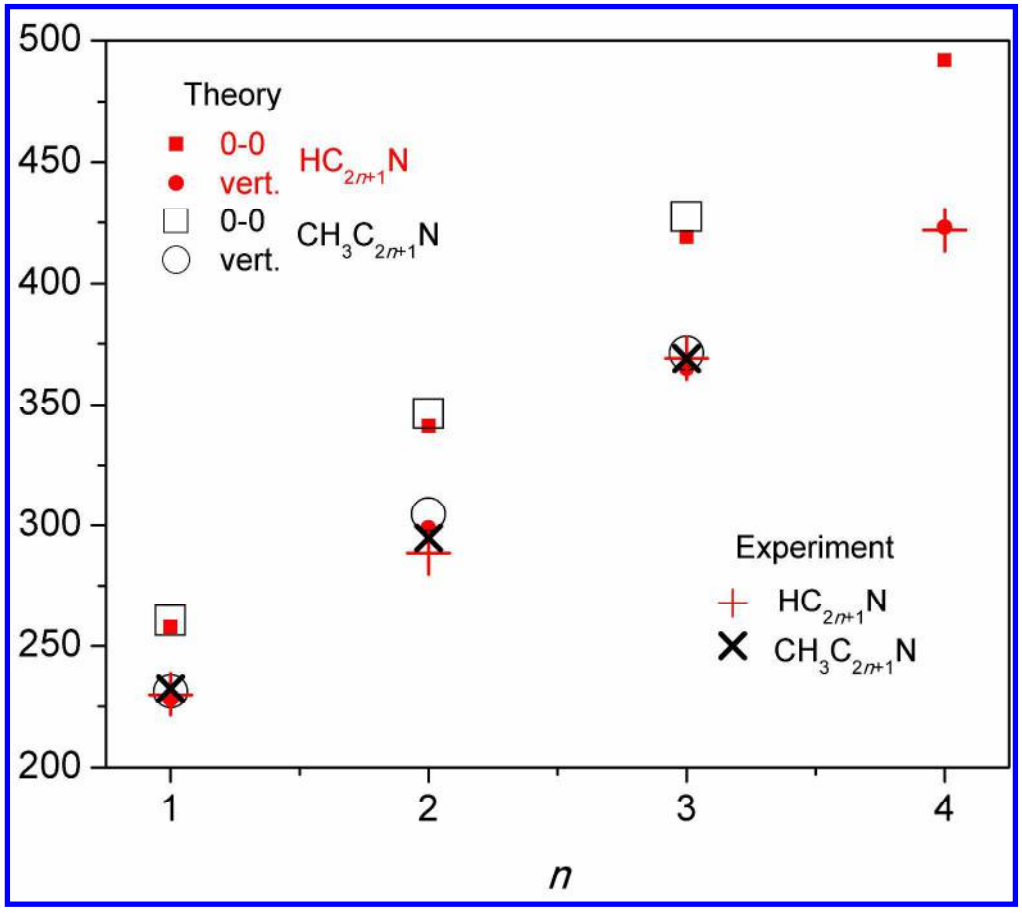

Figure 6.

289x257mm (300 x 300 DPI)

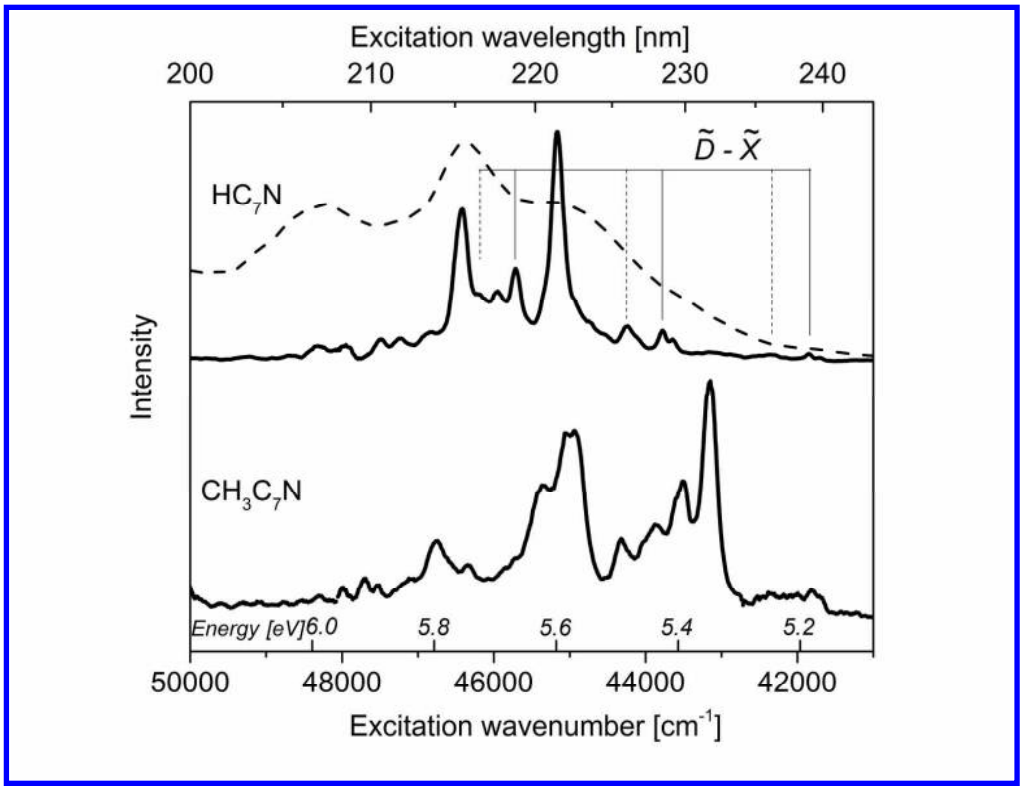

Figure 7.

208x159mm (300 x 300 DPI)

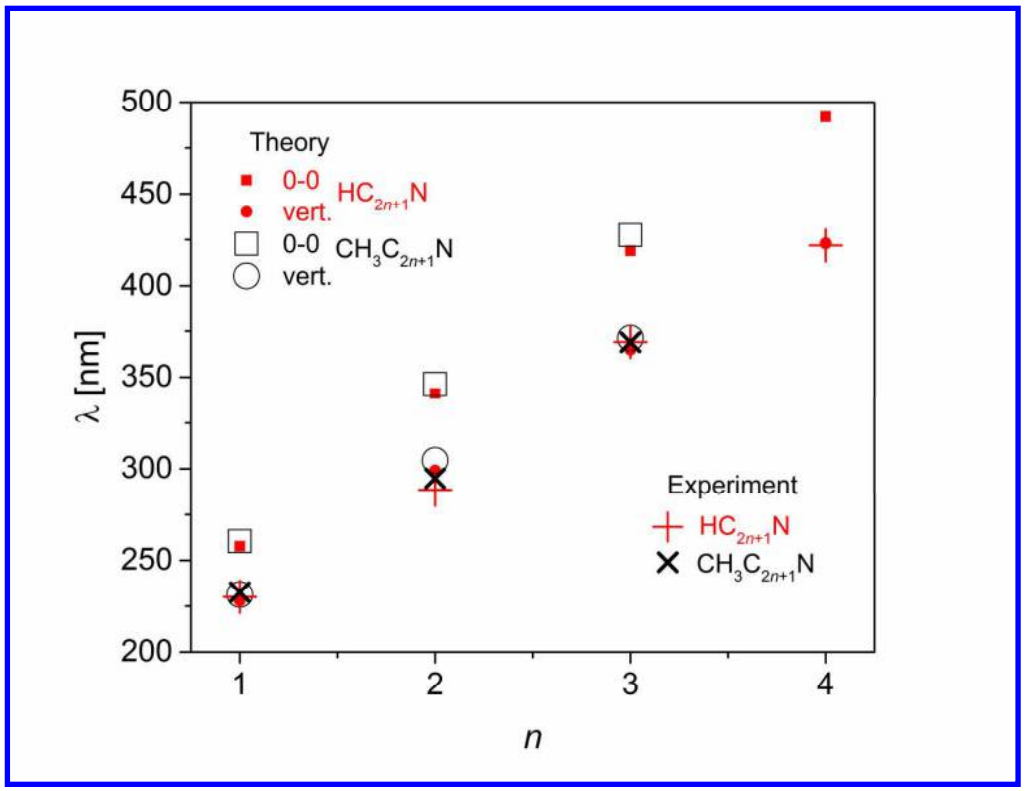

Figure 6.

208x159mm (300 x 300 DPI)